Large-scale shell-model calculations of nuclei around mass 210

E. Teruya,[1,*] K. Higashiyama,[2,†] and N. Yoshinaga[1,‡]
[1]*Department of Physics, Saitama University, Saitama City 338-8570, Japan*
[2]*Department of Physics, Chiba Institute of Technology, Narashino, Chiba 275-0023, Japan*
(Received 8 January 2016; revised manuscript received 2 May 2016; published 30 June 2016)

Large-scale shell-model calculations are performed for even-even, odd-mass, and doubly odd nuclei of Pb, Bi, Po, At, Rn, and Fr isotopes in the neutron deficit region ($Z \geqslant 82$, $N \leqslant 126$) assuming ^{208}Pb as a doubly magic core. All the six single-particle orbitals between the magic numbers 82 and 126, namely, $0h_{9/2}$, $1f_{7/2}$, $0i_{13/2}$, $2p_{3/2}$, $1f_{5/2}$, and $2p_{1/2}$, are considered. For a phenomenological effective two-body interaction, one set of the monopole pairing and quadrupole-quadrupole interactions including the multipole-pairing interactions is adopted for all the nuclei considered. The calculated energies and electromagnetic properties are compared with the experimental data. Furthermore, many isomeric states are analyzed in terms of the shell-model configurations.

DOI: 10.1103/PhysRevC.93.064327

I. INTRODUCTION

The atomic nucleus is a many-body complex system of nucleons. Its structure is determined in terms of the interplay between the single-particle motion of nucleons and their collective motion. It is generally hard to describe the nuclear structure in terms of the nuclear shell model. The shell-model dimension of typical nuclei around mass 130 amounts to more than 10^{11}, which overwhelmingly exceeds the number of configurations tractable with the present computing power. One needs to settle down this problem when the shell model is applied to nuclei above mass 100. For example, the Monte Carlo shell model is one of the promising methods and attracts considerable attention, although it takes a lot of computational time [1,2]. In contrast, the conventional diagonalization approach using the Lanczos diagonalization method requires a truncation of the shell-model space [3]. Nevertheless, few valence-particle systems around doubly magic nuclei are relatively easy to describe in terms of independent nucleons alone. A vast number of shell-model calculations were performed for nuclei in various different regions in the past. In particular, systematic shell-model calculations in medium mass region were carried out assuming the ^{40}Ca core [4], the ^{56}Ni core [5,6], the ^{78}Ni core [7–9], and the ^{132}Sn core [10–16].

The doubly closed nucleus of ^{208}Pb is known to exhibit the aspect of a strong core, which is partly seen in the large first 3^- and 2^+ excitation energies [17]. In recent years, a number of experimental investigations have been carried out in the region around ^{208}Pb with neutron holes and proton particles ($Z \geqslant 82$, $N \leqslant 126$) [18–25]. Energy spectra for high-lying states and new high-spin isomers were observed in several nuclei.

Theoretically, low-lying states in this region are successfully interpreted in terms of a few valence particles in the shell-model configurations. The measured magnetic moments of the isomeric 8^+_1 states in $^{210-214}$Rn are well described by the assignment of the $(\pi h^4_{9/2})$ configuration [26]. Low-lying near-yrast states were analyzed in terms of the interacting boson plus two quasiparticles model [27], where one of the bosons is replaced by a pair of nucleons at high spin [28]. The nucleon pair approximation was also systematically applied for low-lying states of nuclei around ^{208}Pb [29].

In this region, microscopic shell-model calculations for single-closed nuclei were carried out assuming the ^{208}Pb core [30–34] and also for some open-shell nuclei with a few valence particles [35,36]. In the preliminary study [37], the shell-model calculations were carried out for even-even nuclei of Po and Rn isotopes. A phenomenological monopole and quadrupole pairing plus quadrupole-quadrupole interaction was used for the effective interaction. The experimental energy levels of the low-lying states were well reproduced except for the 8^+_1 states, where the level ordering of the 6^+_1 and 8^+_1 states was predicted in reverse.

As described above, there have been already several systematic studies using the shell model. However, the numbers of treated nuclei were limited in most of the studies. Thus the main purpose of the present study is to carry out a systematic study of as many computationally feasible nuclei as possible in the mass around the 210 region, treating even-even, odd-mass, and doubly odd nuclei on the same footing.

In this study the shell-model calculations are performed for even-even, odd-mass, and doubly odd nuclei of $_{82}$Pb, $_{83}$Bi, $_{84}$Po, $_{85}$At, $_{86}$Rn, and $_{87}$Fr isotopes with a few neutron holes and a few proton particles assuming ^{208}Pb as a doubly magic core. As for a phenomenological interaction, one set of the interaction strengths, which consists of the multipole-paring interactions including the monopole pairing and quadrupole-quadrupole interactions, is employed for all the nuclei considered. The energy spectra and electromagnetic properties are calculated and compared with the experimental data. Furthermore, many isomeric states are analyzed in terms of the shell-model configurations.

This paper is organized as follows. The general framework of the present shell-model study is given in Sec. II. Energy levels and electromagnetic properties are presented and compared with the experimental data for each nucleus in Sec. III. Characteristic features of nuclei in this region are analyzed and

*teruya@nuclei.th.phy.saitama-u.ac.jp
†koji.higashiyama@it-chiba.ac.jp
‡yoshinaga@phy.saitama-u.ac.jp

TABLE I. Adopted single-particle energies $\varepsilon_\tau(\tau = \nu$ or $\pi)$ for neutron holes and proton particles (in MeV). The energies for the neutron $0i_{13/2}$ and the proton $0i_{13/2}$ orbitals are changed linearly with numbers of valence neutron holes ($\bar{N}_\nu$) and proton particles (N_π). Definitions of $\epsilon_\nu(i_{13/2})$ and $\epsilon_\pi(i_{13/2})$ are given in the text.

j	$2p_{1/2}$	$1f_{5/2}$	$2p_{3/2}$	$0i_{13/2}$	$1f_{7/2}$	$0h_{9/2}$
ε_ν	0.000	0.570	0.898	$\epsilon_\nu(i_{13/2})$	2.340	3.415
ε_π	3.634	2.826	3.119	$\epsilon_\pi(i_{13/2})$	0.896	0.000

discussed in detail in Sec. IV. Finally this work is summarized in Sec. V.

II. THEORETICAL FRAMEWORK

Systematic studies are carried out for even-even, odd-mass, and doubly odd nuclei with proton particles and neutron holes around the ^{208}Pb nucleus using the full fledged shell model. For single-particle levels, all the six $0h_{9/2}$, $1f_{7/2}$, $0i_{13/2}$, $2p_{3/2}$, $1f_{5/2}$, and $2p_{1/2}$ orbitals in the major shell between the magic numbers 82 and 126 are taken into account for both neutrons and protons. The single-particle energies $\varepsilon_\tau(\tau = \nu$ or $\pi)$ employed in the present calculations are listed in Table I, which are adopted from the experimental energy levels of ^{209}Bi (for proton single-particle energies) and ^{207}Pb (for neutron single-hole energies). As for each neutron or proton $0i_{13/2}$ orbital, it is assumed that the energy of the single-particle orbital changes linearly with the numbers of valence neutron holes and proton particles. They are determined (in MeV) as follows:

$$\epsilon_\nu(0i_{13/2}) = -0.065\bar{N}_\nu + 1.698, \quad (1)$$

$$\epsilon_\pi(0i_{13/2}) = -0.050N_\pi + 1.659, \quad (2)$$

where $\bar{N}_\nu$ and N_π represent the number of valence neutron holes and valence proton particles, respectively. The number dependence of the $0i_{13/2}$ single-particle energies conforms with the experimentally suggested value when $N_\pi = 1$ and $\bar{N}_\nu = 1$. This number dependence is introduced for a better reproduction of the low-lying positive parity states of odd-mass nuclei after adjusting two-body interactions. The necessity of introducing the number dependence is discussed and the effects are analyzed in Sec. IV C.

As an effective interaction, an extended pairing plus quadrupole-quadrupole interaction is employed. The effective shell-model Hamiltonian is given by

$$\hat{H} = \hat{H}_\nu + \hat{H}_\pi + \hat{H}_{\nu\pi}, \quad (3)$$

where $\hat{H}_\nu$, $\hat{H}_\pi$, and $\hat{H}_{\nu\pi}$ represent neutron, proton, and neutron-proton interactions, respectively. The interactions among like nucleons are expressed as

$$\hat{H}_\tau = \hat{H}_{c\tau} + \hat{H}_{h\tau}. \quad (4)$$

The first term $\hat{H}_{c\tau}$ $(\tau = \nu$ or $\pi)$ represents the conventional pairing plus quadrupole interaction, which consists of spherical single-particle energies, the monopole-pairing (MP) interaction, the quadrupole-pairing (QP) interaction,

$$\hat{H}_{c\tau} = \sum_{jm} \varepsilon_{j\tau} c^\dagger_{jm\tau} c_{jm\tau} - G_{0\tau} \hat{P}^{\dagger(0)}_\tau \hat{P}^{(0)}_\tau - G_{2\tau} \hat{P}^{\dagger(2)}_\tau \cdot \hat{\tilde{P}}^{(2)}_\tau. \quad (5)$$

Here $c^\dagger_{jm\tau}$ $(c_{jm\tau})$ is the nucleon creation (annihilation) operator in the orbital $jm\tau$. The second term $\hat{H}_{h\tau}$ in Eq. (4) represents higher-order interactions, which consist of higher multipole-pairing (HMP) interactions,

$$\hat{H}_{h\tau} = -\sum_{L=4,6,8,10} G_{L\tau} \hat{P}^{\dagger(L)}_\tau \cdot \hat{\tilde{P}}^{(L)}_\tau. \quad (6)$$

Here detailed definitions of the interactions are given in Ref. [16].

Only for the proton part, an additional pairing interaction with spin 8 between two protons in the $0h_{9/2}$ and $1f_{7/2}$ orbitals (MP-8), $\hat{H}^{(8)}(\pi h_{9/2} f_{7/2})$, is added to Eq. (4). It is explicitly defined as

$$\hat{H}^{(8)}(\pi h_{9/2} f_{7/2}) = -G^{(8)}_{\pi h_{9/2} f_{7/2}} \hat{P}^{\dagger(8)}_\pi(h_{9/2} f_{7/2}) \cdot \hat{\tilde{P}}^{(8)}_\pi(h_{9/2} f_{7/2}), \quad (7)$$

with

$$\hat{P}^{\dagger(8)}_{M\pi}(h_{9/2} f_{7/2}) = \left[c^\dagger_{h_{9/2}} c^\dagger_{f_{7/2}}\right]^{(8)}_M. \quad (8)$$

Here, two protons in the $0h_{9/2}$ and $1f_{7/2}$ orbitals are coupled with spin 8 and positive parity, which is the maximum spin available between these two orbitals. The necessity of this interaction is discussed and its effects are analyzed in Sec. IV B.

The interaction between neutrons and protons $\hat{H}_{\nu\pi}$ consists of the quadrupole-quadrupole (QQ) interaction, which is given as

$$\hat{H}_{\nu\pi} = -\kappa_{\nu\pi} \hat{Q}_\nu \cdot \hat{Q}_\pi. \quad (9)$$

Harmonic-oscillator states are used as the single-particle basis states with the oscillator parameter $b = \sqrt{\hbar/(M\omega)}$. The adopted two-body interaction strengths are listed in Table II. Only one set of strengths is adopted for all the nuclei.

TABLE II. Strengths of adopted two-body interactions between neutrons (ν-ν) and those between protons (π-π). G_0 and G_2 indicate the strengths of the monopole (MP) and quadrupole-pairing (QP) interactions between like nucleons. G_L $(L = 4,6,8,10)$ denote the strengths for higher multipole-pairing (HMP) interactions between like nucleons. The strength of the proton two-body interaction between the $0h_{9/2}$ and $1f_{7/2}$ orbitals (MP-8) is taken as $G^{(8)}_{\pi h_{9/2} f_{7/2}} = 0.50$. The strength of the $Q_\nu Q_\pi$ interaction between neutrons and protons is taken as $\kappa_{\nu\pi} = -0.060$. The strengths of the MP, HMP, and MP-8 interactions are given in units of MeV. The strengths of the QP and QQ interactions are given in units of MeV/b^4 using the oscillator parameter b.

	G_0	G_2	G_4	G_6	G_8	G_{10}
ν-ν	0.145	0.013	0.500	0.500	1.100	2.000
π-π	0.145	0.013	0.400	0.400	–0.600	0.000

In this region, shell-model dimensions for diagonalization are too large to perform a full calculation without truncation. Thus it is necessary to truncate the shell-model dimension. In this study, the same truncation scheme adopted in Sec. IIB of Ref. [16] is taken for all the nuclei. All calculations are performed with the truncation of $L_c = 500$. Here the definition of L_c is the same as given in Sec. IIB in Ref. [16]. This truncation is found to be sufficient for reproducing low-lying energies and electromagnetic transitions among low lying after checking the effect of truncation by increasing $L_c = 500$ to $L_c = 1000$.

In this paper, $E2$ transition rates, magnetic moments, and quadrupole moments are also calculated. For $E2$ transition rates and quadrupole moments, the effective charges are taken as $e_\nu = -0.85e$ for neutrons and $e_\pi = 1.50e$ for protons. For magnetic moments, the adopted gyromagnetic ratios for orbital angular momenta are $g_{\ell\nu} = 0.00$, $g_{\ell\pi} = 1.00$, and those for spin are $g_{s\nu} = -1.91$ and $g_{s\pi} = 2.79$, which are free-nucleon g factors attenuated by a factor of 0.5. These effective charges and gyromagnetic ratios are adjusted to reproduce the experimental data in single-closed nuclei.

Further details of the shell-model effective interactions and electromagnetic transition operators are presented in Ref. [16].

III. NUMERICAL RESULTS

In this section, the theoretical results are given for each nucleus. The energy spectra, $E2$ transition rates, magnetic moments, and quadrupole moments are calculated. For energy spectra, up to four observed energy levels are shown from the yrast state for each spin and parity in experiment. As for the theoretical states, two levels for each spin and parity from the lowest level are shown in general. If third or fourth states are observed in experiment, third or fourth energy levels are shown in theory.

Characteristic features are discussed for each nucleus. For example, some isomeric states are discussed. There are several reasons why states become isomers. Because of their reasons for existence, they are classified as K isomers, spin-gap isomers, shape isomers, and so on [38]. Many isomers in this region are spin-gap isomers, which do not undertake gamma transitions with low-spin change, such as $E2$ or $M1$ transitions, because of the large spin difference between initial and final states.

A. Pb isotopes

Here $^{203-206}$Pb isotopes are discussed. Figure 1 shows the theoretical energy spectra for even-even Pb isotopes in comparison with the experimental data [39–41]. Not only the yrast states, but also non-yrast states are excellently reproduced. The 3^-_1 states in both ^{206}Pb and ^{204}Pb, which are known to be made by core excitations, are beyond the present framework. Similarly, the 1^- states at 3.744 and 4.329 MeV and 2^- states at 3.980 and 4.317 MeV for ^{206}Pb also are seemingly made by core excitations.

In both nuclei, states whose spin and parity is assigned as 8^+ are not observed experimentally below 4 MeV. From the fact that the experimental 10^+_1 states decay to the 9^-_1 states by the $E1$ transition, the 8^+_1 states might be located above the 10^+_1 states. However, the 8^+_1 states are calculated just below the 10^+_1 states. The 8^+_1 state is calculated at 3.701 MeV (3.311 MeV) for ^{206}Pb (^{204}Pb) in the present model.

Figure 2 shows the theoretical energy spectra for odd-mass Pb isotopes in comparison with the experimental data [39,42,43]. Good agreements with the experimental data are obtained, in particular for the low-lying states with negative parity. The $1/2^+_1$ state for ^{205}Pb is observed at 2.795 MeV. The theoretical $1/2^+_1$ state is calculated at 4.492 MeV in the present model. The experimental $1/2^+_1$ state is seemingly made by core excitations. The configuration is inferred as the 3^-_1 state of the even-even core ^{206}Pb coupled with the neutron $1f_{5/2}$ single-particle state: $(3^-_{\rm core} \otimes \nu f^{-1}_{5/2})$. The $3/2^+$, $5/2^+$, . . ., and $11/2^+$ states with the same configuration are not found in experiment.

Calculated results of the $B(E2)$ values, magnetic moments, and quadrupole moments for Pb isotopes are given in Tables III and IV in comparison with the experimental data [39–44]. Theoretical calculations reproduce the experimental data very well on the whole. Small experimental $B(E2)$ values in ^{205}Pb are not reproduced well. For example, the experimental $B(E2; (21/2^+_1) \to 17/2^+_1)$ value is 0.01694(5) W.u., while the theoretical one is 3.160 W.u. In theory, the $17/2^+_1$ state consists of the $[\nu(f_{5/2})^2_{2^+} i_{13/2}]$ configuration and the $21/2^+_1$ state has the $[\nu(f_{5/2})^2_{4^+} i_{13/2}]$ configuration. This is why the theoretical $B(E2; 21/2^+_1 \to 17/2^+_1)$ value is large. The experimental spin-parity confirmation of the $(21/2^+_1)$ state might be required.

In ^{206}Pb, the sign of the magnetic moment of the 6^-_1 state is positive and that of the 7^-_1 state is negative in experiment. The signs of these values are negative in the present calculation. Both the 6^-_1 and 7^-_1 states consist of the $(\nu p^{-1}_{1/2} i^{-1}_{13/2})$ configuration and both states should have the same sign in theory. The magnetic moments of the 6^-_1 and 7^-_1 states were also calculated in Ref. [32] using the shell model and signs of both magnetic moments are also negative. Their results are consistent with ours.

B. Bi isotopes

Here $^{204-208}$Bi isotopes are discussed. Figure 3 shows the theoretical energy spectra for odd-mass Bi isotopes in comparison with the experimental data [39,43,45]. Theoretical calculations reproduce the experimental data well on the whole. In these nuclei, large differences between experiment and theory are seen in energies of the $1/2^+_1$ and $3/2^+_1$ states. It was inferred that the $1/2^+_1$ state belongs to the $(\pi h^2_{9/2} s^{-1}_{1/2})$ configuration in these nuclei [46]. Here the proton $2s_{1/2}$ hole orbital below the magic number 82 is not included in the present framework. It was also mentioned that the $3/2^+_1$ state for ^{207}Bi mainly consists of the $(\nu p^{-2}_{1/2} \pi h^2_{9/2} d^{-1}_{3/2})$ configuration with a small amount of the $(\nu p^{-2}_{1/2} \pi h_{9/2} \otimes 3^-)$ configuration [39,47]. Likewise, the proton $1d_{3/2}$ hole orbital below the magic number 82 is not included in the present framework.

Figure 4 shows the theoretical energy spectra for doubly odd Bi isotopes in comparison with the experimental

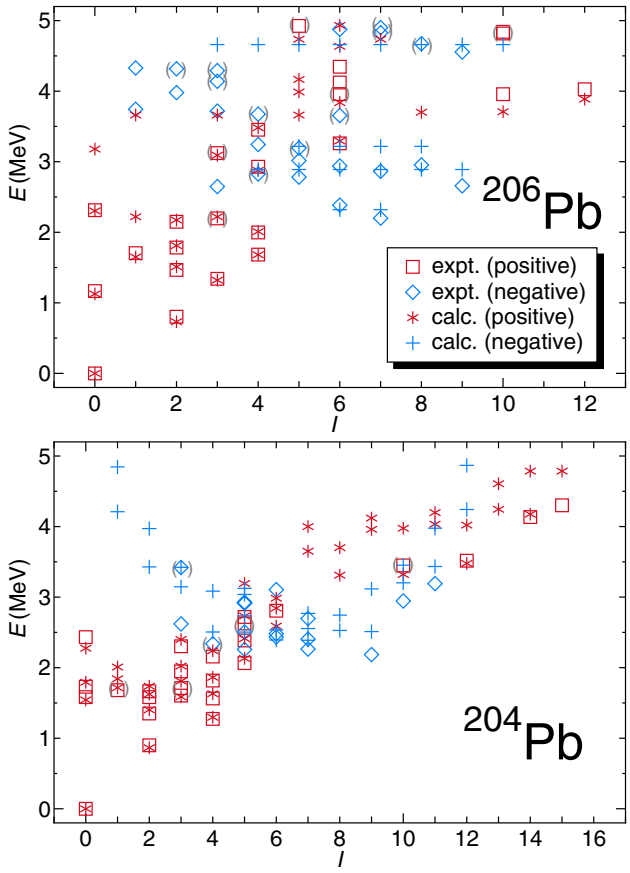

FIG. 1. Theoretical energy spectra for even-even Pb isotopes in comparison with the experimental data. The squares and diamonds represent experimental positive and negative parity states, respectively. The asterisks and crosses represent theoretical positive and negative parity states, respectively. The experimental data are taken from Refs. [39–41]. Ambiguous states are shown with parentheses.

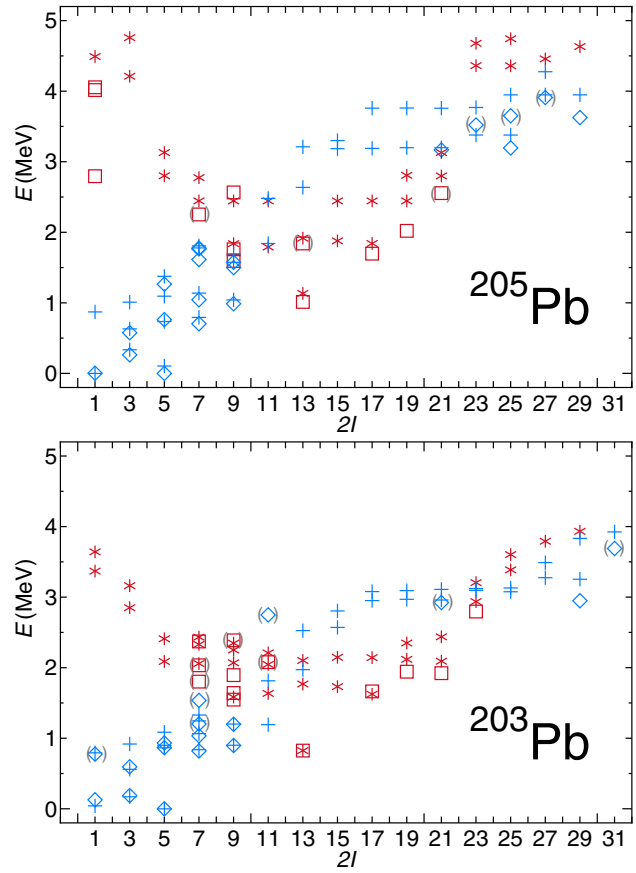

FIG. 2. Same as Fig. 1, but for odd-mass Pb isotopes. The experimental data are taken from Refs. [39,42,43].

data [17,23,39–41]. In ^{208}Bi, which is a one-neutron-hole and one-proton-particle system, energies of low-lying states below 1.5 MeV are well reproduced. The 12^+_2, 13^+_2 states and states with spin over 14 (irrespective of its parity) are beyond the present framework. The 12^+_1 and 13^+_1 states, which consist of the $(\nu i^{-1}_{13/2}\pi i_{13/2})$ configuration, are well reproduced in the present model.

In ^{208}Bi, the 2^-_1, 3^-_1, ..., and 11^-_1 states are members of the $(\nu i^{-1}_{13/2}\pi h_{9/2})$ configuration. The observed 2^-_1 and 11^-_1 states are higher than other members. However, the theoretical calculation fails in reproducing this situation. This problem was also seen in the previous calculation for ^{132}Sb [16]. This nucleus is a one-neutron-hole and one-proton-particle system assuming the ^{132}Sn core, which is a similar system as ^{208}Bi. In ^{132}Sb, the 2^-_1, 3^-_1, ..., and 9^-_1 states with the $(\nu h^{-1}_{11/2}\pi g_{7/2})$ configuration are seen in the low-lying states and the 2^-_1 and 9^-_1 states are located at high energies than other members. A shell-model calculation was performed for ^{132}Sb in the same framework. It was found that a hexadecapole interaction among alike nucleons is important to reproduce these negative parity states [16].

Through the argument in the above, a hexadecapole interaction between neutrons and protons would be necessary to well reproduce energies of the 2^-_1 and 11^-_1 states in ^{208}Bi. However, a large amount of computational resources are required for the introduction of hexadecapole-hexadecapole interactions between alike nucleons. Thus these kinds of higher multipole-multipole interactions are not introduced in this study.

Similar to ^{208}Bi, the theoretical 11^-_1 states in ^{206}Bi and ^{204}Bi are calculated lower than the experimental 11^-_1 states. Theoretical 11^-_1 states in ^{206}Bi and ^{204}Bi would be reproduced at observed positions of the experimental 11^-_1 states by introducing such a hexadecapole interaction. In fact, a shell-model calculation [23] was carried out for ^{206}Bi using the interaction deduced from the Hamada-Johnston potential and the 11^-_1 state was calculated at 1.716 MeV (1.639 MeV in experiment).

Calculated results of the $B(E2)$ values, magnetic moments, and quadrupole moments for Bi isotopes are given in Tables V and VI in comparison with the experimental data [17,39–41,43,45]. The small $B(E2; 4^+_1 \rightarrow 6^+_1)$ value in ^{206}Bi is well reproduced. The quadrupole moments of the 10^-_1 states for ^{206}Bi and ^{204}Bi are small in experiment [0.049(9) eb for ^{206}Bi and 0.063(12) eb for ^{204}Bi]. However, the present results fail in reproducing these experimental data (-0.225 eb for ^{206}Bi and -0.299 eb for ^{204}Bi). It is, however, noted that the

TABLE III. Comparison between the experimental $B(E2)$ values (Expt.) and the theoretical results (Calc.) for Pb isotopes (in W.u.). The experimental data are taken from Refs. [39–43].

^{206}Pb	Expt.	Calc.
$2_1^+ \to 0_1^+$	2.80(9)	2.939
$4_1^+ \to 2_1^+$		3.160
$6_1^+ \to 4_1^+$		1.931
$8_1^+ \to 6_1^+$		0.324
$12_1^+ \to 10_1^+$	0.34(6)	0.281
$6_1^- \to 7_1^-$	$0.08\ ^{+31}_{-8}$	0.064
^{204}Pb	Expt.	Calc.
$2_1^+ \to 0_1^+$	4.69(5)	4.262
$4_1^+ \to 2_1^+$	0.00382(9)	0.062
$6_1^+ \to 4_1^+$		0.089
$8_1^+ \to 6_1^+$		0.002
$0_2^+ \to 2_1^+$	0.81(25)	0.078
$7_1^- \to 5_1^-$	∼0.6	0.064
$7_1^- \to 9_1^-$	$0.15\ ^{+4}_{-6}$	0.004
^{205}Pb	Expt.	Calc.
$1/2_1^- \to 5/2_1^-$	0.0108(4)	0.199
$3/2_1^- \to 5/2_1^-$		1.095
$3/2_1^- \to 1/2_1^-$		0.032
$7/2_1^- \to 5/2_1^-$		3.960
$7/2_1^- \to 3/2_1^-$		0.003
$25/2_1^- \to 21/2_1^-$	0.053(10)	0.282
$29/2_1^- \to 25/2_1^-$	0.7317(20)	1.021
$17/2_1^+ \to 13/2_1^+$	0.13009(20)	2.618
$19/2_1^+ \to 17/2_1^+$	∼0.14	0.004
$21/2_1^+ \to 17/2_1^+$	0.01694(5)	3.160
^{203}Pb	Expt.	Calc.
$1/2_1^- \to 5/2_1^-$	0.96(6)	0.792
$3/2_1^- \to 5/2_1^-$		0.306
$3/2_1^- \to 1/2_1^-$		0.032
$7/2_1^- \to 5/2_1^-$		3.125
$7/2_1^- \to 3/2_1^-$		0.781
$21/2_1^+ \to 17/2_1^+$	0.139(10)	0.029

magnetic moments of the same states are well reproduced. This phenomenon is discussed in Sec. IV A.

C. Po isotopes

Here $^{205-210}$Po isotopes are discussed. Figure 5 shows the theoretical energy spectra for even-even Po isotopes in comparison with the experimental data [17,39,41,48].

^{210}Po is a system with two valence protons. The energy gap between the 8_1^+ and 10_1^+ states is large in this nucleus. This is because the 8_1^+ state is constructed by two protons in the $0h_{9/2}$ orbital. The 0_1^+, 2_1^+, 4_1^+, and 6_1^+ states are also constructed by the $(\pi h_{9/2}^2)$ configuration. In contrast, two protons need to occupy the $0i_{13/2}$ orbital to make states over 10^+. The 1_1^+, 2_2^+, 3_1^+, 4_2^+, 5_1^+, 6_2^+, 7_1^+, and 8_2^+ states are members of the $(\pi h_{9/2} f_{7/2})$ configuration.

In ^{210}Po, the 11_1^- state consists of the $(\pi h_{9/2} i_{13/2})$ configuration. The 11_2^- state and states with spin greater than 13 are beyond the present framework. Except for these states, theoretical calculations reproduce the experimental data well for all the nuclei.

TABLE IV. Comparison of the magnetic dipole moments μ (in μ_N) and the electric quadrupole moments Q (in eb) obtained by the shell model (Calc.) to the experimental data (Expt.) for Pb isotopes. The experimental data are taken from Refs. [39–44].

^{206}Pb	μ		Q	
	Expt.	Calc.	Expt.	Calc.
2_1^+	<0.030	+0.056	+0.05(9)	+0.282
4_1^+		+0.413		+0.328
6_1^+		−0.263		+0.358
8_1^+		−1.156		+0.037
12_1^+	−1.795(22)	−1.763	0.51(2)	+0.468
7_1^-	−0.152(3)	−0.637	0.33(5)	+0.304
6_1^-	+0.8(4)	−1.217		+0.294
^{204}Pb	Expt.	Calc.	Expt.	Calc.
2_1^+	<0.02	+0.043	+0.23(9)	−0.052
4_1^+	+0.224(3)	+0.210	0.44(2)	+0.462
6_1^+		+0.691		+0.381
8_1^+		−1.154		+0.037
^{205}Pb	Expt.	Calc.	Expt.	Calc.
$1/2_1^-$		+0.319		
$3/2_1^-$		−0.665		+0.134
$5/2_1^-$	+0.7117(4)	+0.594	+0.226(37)	+0.206
$7/2_1^-$		+0.535		+0.148
$9/2_1^-$		+0.617		+0.423
$13/2_1^+$	−0.975(40)	−0.954	0.30(5)	+0.214
^{203}Pb	Expt.	Calc.	Expt.	Calc.
$1/2_1^-$		+0.319		
$3/2_1^-$		−0.780		+0.137
$5/2_1^-$	+0.6864(5)	+0.601	+0.095(52)	+0.066
$7/2_1^-$		+0.182		−0.073
$9/2_1^-$		+0.592		+0.021
$13/2_1^+$		−0.953		+0.165
$21/2_1^+$	−0.641(21)	−0.775		+0.715

Figure 6 shows the theoretical energy spectra for odd-mass Po isotopes in comparison with the experimental data [39,43,45,49]. In ^{209}Po, a large energy difference between the calculated $21/2_1^-$ and $23/2_1^-$ states is seen. It is noted that no experimentally confirmed $23/2_1^-$ state is observed. The $21/2_1^-$ state mainly consists of the $(\nu f_{5/2}^{-1} \pi h_{9/2}^2)$ configuration. In contrast, the $23/2_1^-$ state mainly consists of the $(\nu f_{7/2}^{-1} \pi h_{9/2}^2)$ configuration. This difference of the two configurations causes the large energy gap between the $21/2_1^-$ and $23/2_1^-$ states.

The $19/2_1^-$ states are spin-gap isomers with long half-lives of 2.79(8) s and 57.4(9) ms for ^{207}Po and ^{205}Po, respectively [39]. These states mainly decay to the $13/2_1^+$ states by the $E3$ transition. From this fact, the $15/2^-$ and $17/2^-$ states which can be connected to the $19/2_1^-$ state by the $E2$ or $M1$ transitions, should be located above the $19/2_1^-$ state. In theory, however, the $15/2^-$ and $17/2^-$ states are calculated slightly lower than the $19/2_1^-$ states in both nuclei.

The calculated $B(E2)$ values, magnetic moments, and quadrupole moments for Po isotopes are given in Tables VII and VIII in comparison with the experimental

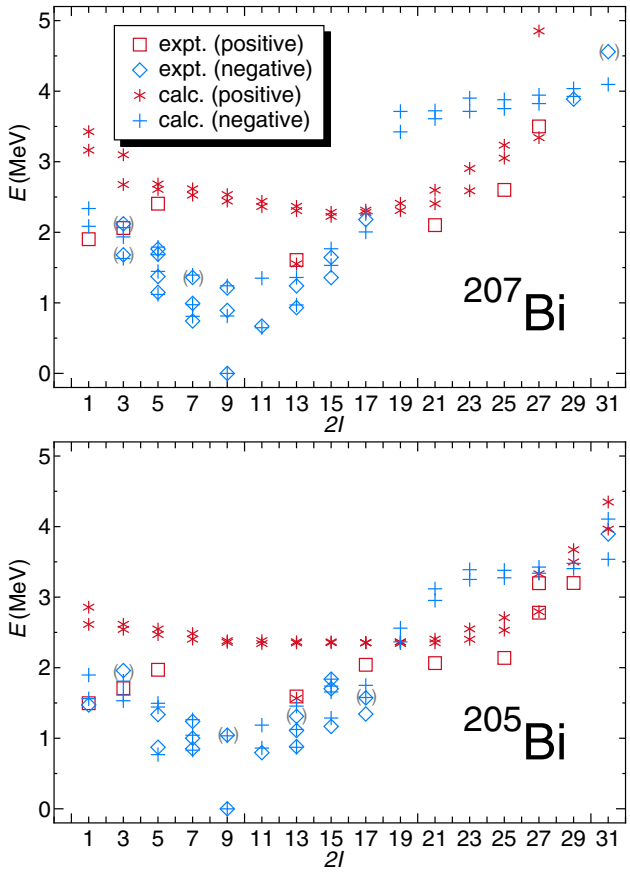

FIG. 3. Same as Fig. 1, but for odd-mass Bi isotopes. The experimental data are taken from Refs. [39,43,45].

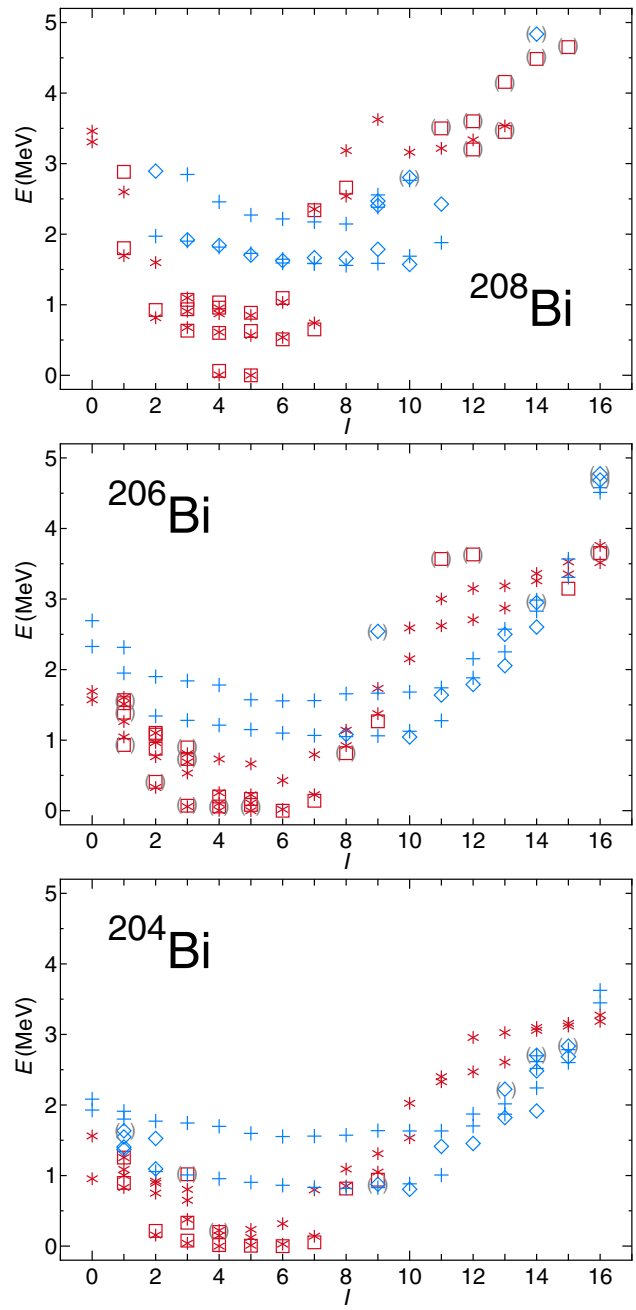

FIG. 4. Same as Fig. 1, but for doubly odd Bi isotopes. The experimental data are taken from Refs. [17,23,39–41].

data [17,39,41,43,45,48,49]. In ^{210}Po, the $E2$ transition rates among the yrast states are successfully reproduced except for the $B(E2;2_1^+ \to 0_1^+)$ value. The experimental $B(E2;2_1^+ \to 0_1^+)$ value is 0.56(12) W.u. In contrast the theoretical $B(E2;2_1^+ \to 0_1^+)$ value is 4.12 W.u. This $B(E2)$ value was also calculated using the shell model and was given as 3.55 W.u. [33,34].

The experimental magnetic moments and quadrupole moments are well reproduced by the present calculation. Only one disagreement is seen in the magnetic moment of the $1/2_1^-$ state for ^{209}Po, which is calculated almost half the value of the experimental value.

D. At isotopes

Here $^{206-211}$At isotopes are discussed. Figure 7 shows the theoretical energy spectra for odd-mass At isotopes in comparison with the experimental data [39,45,49,50]. In these nuclei, low-lying negative parity states are excellently reproduced.

It is noticed from Fig. 7 that the energy of the $19/2_1^-$ state is higher compared to other first negative parity states in these nuclei. For example, in ^{211}At, the $17/2_1^-$ and $21/2_1^-$ states are calculated at 1.356 and 1.496 MeV, respectively. In contrast, the $19/2_1^-$ state is calculated at 2.032 MeV. The $17/2_1^-$ and $21/2_1^-$ states consist of the $(\pi h_{9/2}^3)$ configuration. In contrast the $19/2_1^-$ state consists of the $(\pi h_{9/2}^2 f_{7/2})$ configuration. Because the single-particle energy of the $1f_{7/2}$ orbital is higher than that of the $0h_{9/2}$ orbital, the energy of the $19/2_1^-$ state is higher compared to the $17/2_1^-$ and $21/2_1^-$ states. It should be noted that the $19/2^-$ state cannot be constructed by the $(\pi h_{9/2}^3)$ configuration.

The $29/2_1^+$ state at 2.429 MeV in ^{209}At is an isomer with a half-life of 0.916(10) μs [39]. This state is a spin-gap isomer, which decays to the $23/2_1^-$ state at 1.852 MeV by the $E3$ transition. The $29/2_1^+$ state mainly consists of the $[\pi(h_{9/2}^2)_{8^+} i_{13/2}]$ configuration for the proton part, while two

TABLE V. Same as Table III, but for Bi isotopes. The experimental data are taken from Refs. [17,39–41,43,45].

^{207}Bi	Expt.	Calc.
$11/2^-_1 \to 9/2^-_1$		6.099
$7/2^-_1 \to 9/2^-_1$		1.040
$7/2^-_1 \to 11/2^-_1$		0.432
^{205}Bi	Expt.	Calc.
$11/2^-_1 \to 9/2^-_1$		6.995
$7/2^-_1 \to 9/2^-_1$		1.266
$7/2^-_1 \to 11/2^-_1$		0.016
$25/2^+_1 \to 21/2^+_1$	0.58(8)	0.526
^{208}Bi	Expt.	Calc.
$6^+_1 \to 4^+_1$	0.10(3)	0.169
$6^+_1 \to 5^+_1$	1.5(5)	2.013
$7^+_1 \to 5^+_1$	≤0.017	0.848
$4^+_1 \to 5^+_1$		0.576
^{206}Bi	Expt.	Calc.
$4^+_1 \to 6^+_1$	0.0180(6)	0.025
$3^+_1 \to 4^+_1$		4.159
$5^+_1 \to 4^+_1$		3.013
$5^+_1 \to 6^+_1$		0.017
^{204}Bi	Expt.	Calc.
$5^+_1 \to 6^+_1$		4.155
$4^+_1 \to 6^+_1$		0.693
$4^+_1 \to 5^+_1$		4.263

TABLE VI. Same as Table VI, but for Bi isotopes. The experimental data are taken from Refs. [17,39,39–41,43,45].

^{207}Bi	μ		Q	
	Expt.	Calc.	Expt.	Calc.
$7/2^-_1$		+3.648		–0.592
$9/2^-_1$	+4.0915(9)	+3.669	−0.545(38)	–0.717
$11/2^-_1$		+3.477		–0.434
$13/2^-_1$		+3.742		–0.224
$21/2^+_1$	+3.41(6)	+2.494	0.044(8)	–0.056
^{205}Bi	Expt.	Calc.	Expt.	Calc.
$7/2^-_1$		+3.997		–0.638
$9/2^-_1$	+4.065(7)	+3.666	−0.585(43)	–0.763
$11/2^-_1$		+3.345		–0.497
$13/2^-_1$		+3.726		–0.777
$21/2^+_1$	2.70(4)	+1.797		+0.288
$25/2^+_1$	3.21(5)	+2.713		–0.140
^{208}Bi	Expt.	Calc.	Expt.	Calc.
4^+_1		+3.712		–0.508
5^+_1	+4.578(13)	+3.819	−0.51(7)	–0.541
6^+_1		+3.916		–0.313
10^-_1	2.672(14)	+2.379		–0.006
^{206}Bi	Expt.	Calc.	Expt.	Calc.
4^+_1		+3.280		–0.512
5^+_1		+3.653		–0.561
6^+_1	+4.361(8)	+3.784	−0.39(4)	–0.664
10^-_1	2.644(14)	+2.259	0.049(9)	–0.225
^{204}Bi	Expt.	Calc.	Expt.	Calc.
4^+_1		+3.763		–0.651
5^+_1		+3.592		–0.603
6^+_1	+4.322(15)	+3.167	−0.49(15)	–0.511
10^-_1	2.36(23)	+2.269	0.063(12)	–0.298

neutrons mainly couple to spin zero. In this configuration, the maximum spin is 29/2. As one of our empirical rules, using the effective interactions among like nucleons adopted in the present framework, the maximum-spin state among members with one specific configuration is likely to get lower in energy than other members with the same configuration. Accordingly, it is likely that the state which has the maximum spin among those states with the same configuration becomes a spin-gap isomer. In this case, the maximum spin of the $[\pi(h^2_{9/2})_{8^+} i_{13/2}]$ configuration is 29/2. Thus this state gets lower in energy than other states with the same members and becomes a spin-gap isomer. This isomer was also analyzed in Ref. [51] and they suggested the same configuration.

Figure 8 shows the theoretical energy spectra for doubly odd At isotopes in comparison with the experimental data [17,39,41,48]. In ^{206}At, relative energies between the ground state and the 7^+_1 state and also the states above are not known in experiment. In Fig. 8, the excitation energy of the 7^+_1 state is assumed as 0.09 MeV. Almost all states observed in ^{210}At are well reproduced in theory. Furthermore, low-lying positive parity states, which are densely located below 0.2 MeV, are well reproduced in ^{208}At.

The 15^-_1 state at 2.549 MeV in ^{210}At is a spin-gap isomer. The half-life of this state is 0.482(6) μs and this state decays to the 12^+ states by the $E3$ transition [39]. This state mainly consists of the $[\nu p^{-1}_{1/2} \pi(h^2_{9/2})_{8^+} i_{13/2}]$ configuration and spin 15 is the maximum spin made by this configuration. The 13^-_1 and 14^-_1 states, which can be connected to the 15^-_1 state by the $E2$ or $M1$ transitions, are located slightly higher than the 15^-_1 state and the theoretical calculation reproduces this experimental situation. The same configuration was also proposed in Ref. [18].

The 10^-_1 state [47.8(10) ns] and 16^-_1 state [1.5(2) μs] in ^{208}At and the 10^-_1 state [410(80) ns] in ^{206}At are also isomers [39]. These states decay to lower states by $E3$ or $E1$ transitions. In theory, states which can be connected to these isomeric states by the $E2$ or $M1$ transitions are calculated almost degenerately in energy with the isomeric states. Typical energy gaps are around 0.05 MeV.

Calculated results of the $B(E2)$ values, magnetic moments, and quadrupole moments for At isotopes are given in Tables IX and X in comparison with the experimental data [17,39,41,45,48–50]. The experimental data are well reproduced on the whole. In ^{211}At, the large $B(E2; 3/2^-_1 \to 5/2^-_1)$ value is well reproduced. The $B(E2; 3/2^-_1 \to 5/2^-_1)$ value is 32 times larger than the $B(E2; 3/2^-_1 \to 7/2^-_1)$ value. The $3/2^-_1$ and $5/2^-_1$ states consist of the $(\pi h^3_{9/2})$ configuration. In contrast, the $7/2^-_1$ state mainly consists of the $(\pi h^2_{9/2} f_{7/2})$ configuration. It is this difference of the configurations that appears in different magnitudes of the $B(E2; 3/2^-_1 \to 5/2^-_1)$ and $B(E2; 3/2^-_1 \to 7/2^-_1)$ values.

The experimental $B(E2; 3/2^-_1 \to 7/2^-_2)$ value is 4.5 times larger than the $B(E2; 3/2^-_1 \to 7/2^-_1)$ value in ^{211}At. However,

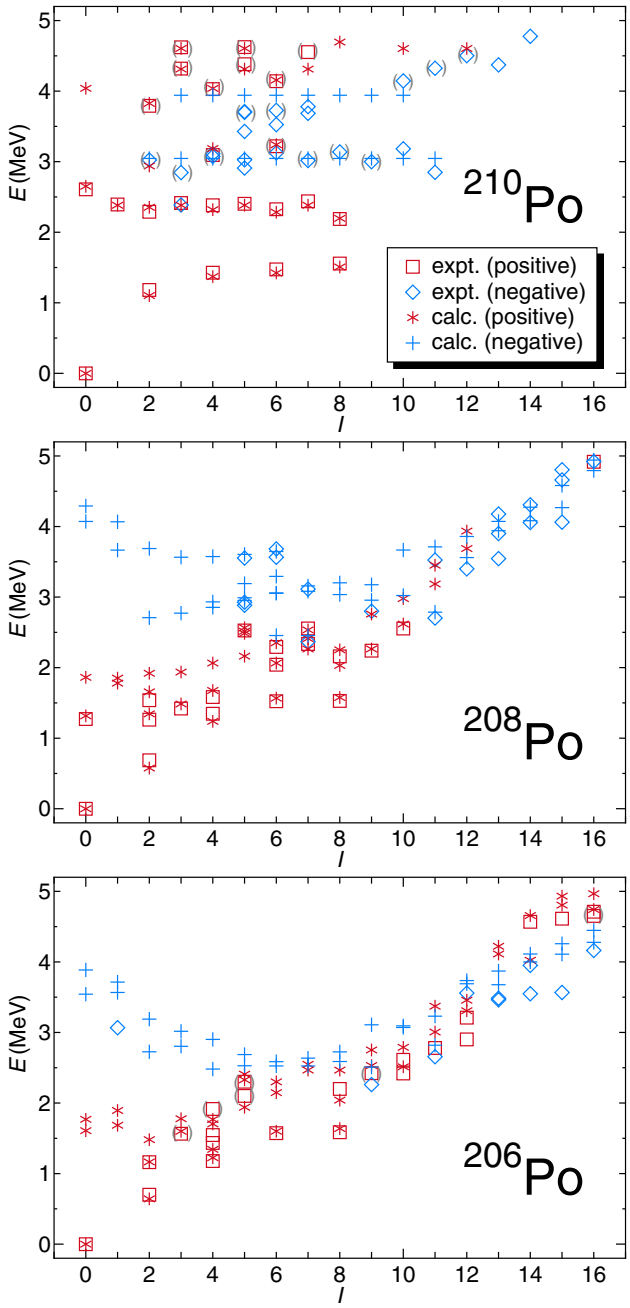

FIG. 5. Same as Fig. 1, but for even-even Po isotopes. The experimental data are taken from Refs. [17,39,41,48].

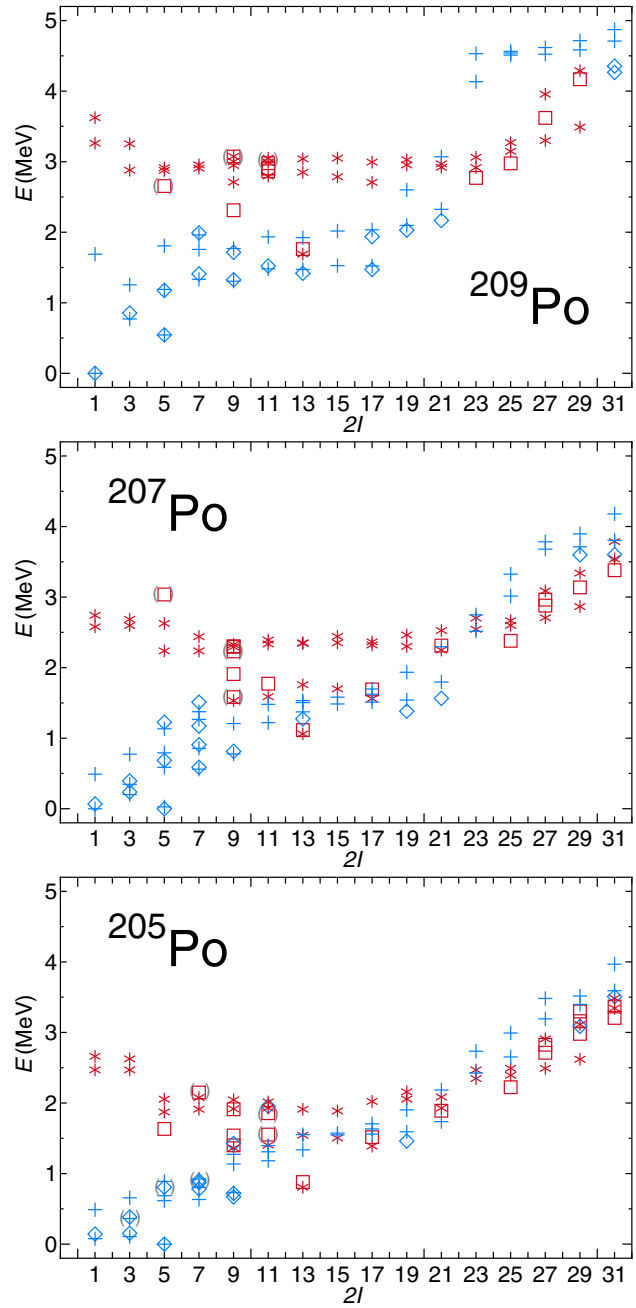

FIG. 6. Same as Fig. 1, but for odd-mass Po isotopes. The experimental data are taken from Refs. [39,43,45,49].

theoretical results give almost the same values for both transition rates. It might be explained by the admixture of the states of the $7/2_1^-$ and $7/2_2^-$ states. Suppose that the original $7/2_1^-$ and $7/2_2^-$ states are admixed as follows:

$$|\widetilde{7/2_1^-}\rangle = \alpha|7/2_1^-\rangle + \sqrt{1-\alpha^2}|7/2_2^-\rangle, \quad (10)$$

$$|\widetilde{7/2_2^-}\rangle = \sqrt{1-\alpha^2}|7/2_1^-\rangle - \alpha|7/2_2^-\rangle. \quad (11)$$

Here, $|\ \rangle$ represents an eigenstate and $|\widetilde{\ }\rangle$ represents an admixed state. If $\alpha = 0.95$ is assumed, the revised transition rates by the admixed states are changed as $B(E2; 3/2_1^- \to \widetilde{7/2_1^-}) =$ 0.36 W.u. [0.40(4) W.u. in experiment] and $B(E2; \widetilde{3/2_1^-} \to \widetilde{7/2_2^-}) = 1.34$ W.u. [1.78(18) W.u. in experiment].

The experimental magnetic moments and quadrupole moments are excellently reproduced by the calculation. This calculation will be helpful to determine signs of these moments.

E. Rn isotopes

Here $^{207-212}$Rn isotopes are discussed. Figure 9 shows the theoretical energy spectra for even-even Rn isotopes in

TABLE VII. Same as Table III, but for Po isotopes. The experimental data are taken from Refs. [17,39,41,43,45,48,49].

^{210}Po	Expt.	Calc.
$2_1^+ \to 0_1^+$	0.56(12)	4.123
$4_1^+ \to 2_1^+$	4.46(18)	4.453
$6_1^+ \to 4_1^+$	3.05(9)	3.028
$8_1^+ \to 6_1^+$	1.12(4)	1.055
$10_1^+ \to 8_1^+$		<0.001
^{208}Po	Expt.	Calc.
$2_1^+ \to 0_1^+$		8.890
$4_1^+ \to 2_1^+$		11.216
$6_1^+ \to 4_1^+$	5.6(4)	6.807
$8_1^+ \to 6_1^+$	6.4(5)	1.684
$10_1^+ \to 8_1^+$		2.206
^{206}Po	Expt.	Calc.
$2_1^+ \to 0_1^+$		12.997
$4_1^+ \to 2_1^+$		11.151
$6_1^+ \to 4_1^+$		5.569
$8_1^+ \to 6_1^+$	2.45(16)	3.829
$10_1^+ \to 8_1^+$		5.121
^{209}Po	Expt.	Calc.
$5/2_1^- \to 1/2_1^-$	2.2(7)	3.691
$3/2_1^- \to 1/2_1^-$		5.206
$3/2_1^- \to 5/2_1^-$		1.298
$13/2_1^- \to 9/2_1^-$	4.37(10)	4.538
$17/2_1^- \to 13/2_1^-$	1.43(5)	1.376
$11/2_1^- \to 7/2_1^-$	13(5)	4.344
$11/2_1^- \to 9/2_1^-$	15(12)	0.172
^{207}Po	Expt.	Calc.
$1/2_1^- \to 5/2_1^-$	0.60(3)	0.912
$3/2_1^- \to 5/2_1^-$		4.697
$3/2_1^- \to 1/2_1^-$		0.083
$7/2_1^- \to 5/2_1^-$		10.999
$7/2_1^- \to 3/2_1^-$		0.096
^{205}Po	Expt.	Calc.
$1/2_1^- \to 5/2_1^-$	0.16(3)	3.586
$3/2_1^- \to 5/2_1^-$		2.048
$3/2_1^- \to 1/2_1^-$		0.196
$7/2_1^- \to 5/2_1^-$		11.022
$7/2_1^- \to 3/2_1^-$		2.603
$9/2_1^- \to 5/2_1^-$		11.960
$25/2_1^+ \to 21/2_1^+$	0.9(3)	0.707

TABLE VIII. Same as Table VI, but for Po isotopes. The experimental data are taken from Refs. [17,39,41,43,45,48,49].

^{210}Po	μ		Q	
	Expt.	Calc.	Expt.	Calc.
2_1^+		+1.718		+0.186
4_1^+		+3.368		+0.134
6_1^+	5.48(5)	+5.038		−0.141
8_1^+	+7.13(5)	+6.734	−0.552(20)	−0.551
11_1^-	+12.20(9)	+11.163	−0.86(11)	−0.965
^{208}Po	Expt.	Calc.	Expt.	Calc.
2_1^+		+0.521		+0.458
4_1^+		+2.398		+0.435
6_1^+	+5.3(6)	+4.780		−0.087
8_1^+	+7.37(5)	+6.617	0.90(4)	−0.926
^{206}Po	Expt.	Calc.	Expt.	Calc.
2_1^+		+0.636		+0.203
4_1^+		+1.364		+0.617
6_1^+		+4.760		−0.256
8_1^+	+7.34(7)	+6.541	1.02(4)	−0.974
^{209}Po	Expt.	Calc.	Expt.	Calc.
$1/2_1^-$	0.68(8)	+0.315		
$3/2_1^-$		−0.342		+0.223
$5/2_1^-$		+0.901		+0.326
$13/2_1^-$	6.13(9)	+5.243	0.126(5)	−0.130
$17/2_1^-$	7.75(5)	+6.718	0.659(7)	−0.703
$13/2_1^+$		−0.931		+0.529
^{207}Po	Expt.	Calc.	Expt.	Calc.
$1/2_1^-$		+0.315		
$3/2_1^-$		−0.529		+0.124
$5/2_1^-$	0.79(6)	+0.643		+0.357
$13/2_1^+$	−0.910(14)	−0.931		+0.577
$25/2_1^+$	5.41(4)	+4.921		−0.400
^{205}Po	Expt.	Calc.	Expt.	Calc.
$1/2_1^-$		+0.308		
$3/2_1^-$		−0.624		+0.274
$5/2_1^-$	+0.76(6)	+0.633		+0.189
$13/2_1^+$	−0.95(5)	−0.935		+0.506

comparison with the experimental data [17,19,39,48,52]. Just like ^{206}At, the relative positions between the ground state and many excited states are not known in ^{210}Rn. The lowest state [the (8_1^+) state] of these excited states is observed at $1.665+x$ MeV. In this figure, this state is shown with an assumption of $x = 0.096$ MeV.

The theoretical energy levels in ^{212}Rn as a whole are slightly lower than the experimental ones, but one-to-one correspondence of energy levels between experiment and theory is well established in these nuclei. One of the features in even-even Rn nuclei is seen in the small energy gap between the 6_1^+ and 8_1^+ states. Because of these small energy gaps, the 8_1^+ states are isomers with half-lives of 0.91(3) μs, 644(40) ns, and 487(12) ns for ^{212}Rn, ^{210}Rn, and ^{208}Rn, respectively [17,48,52]. Theoretical calculations well reproduce the feature of these small energy gaps.

Figure 10 shows the theoretical energy spectra for odd-mass Rn isotopes in comparison with the experimental data [39,45,49,50]. The relative positions between the ground state and many excited states are not known in ^{211}Rn. The lowest state [the $(17/2_1^-)$ state] of these excited states is observed at $1.578+x$ MeV. In this figure, this state is shown with an assumption of $x = 0.050$ MeV. Low-lying negative parity states are excellently reproduced.

Calculated results of the $B(E2)$ values, magnetic moments, and quadrupole moments for Rn isotopes are given in Tables XI and XII in comparison with the experimental data [17,39,45,48–50,52]. Theoretical results reproduce small $B(E2; 14_1^+ \to 12_1^+)$ values for ^{212}Rn and ^{210}Rn. In ^{212}Rn, the 12_1^+ state consists of the $(\pi h_{9/2}^4)$ configuration. In contrast,

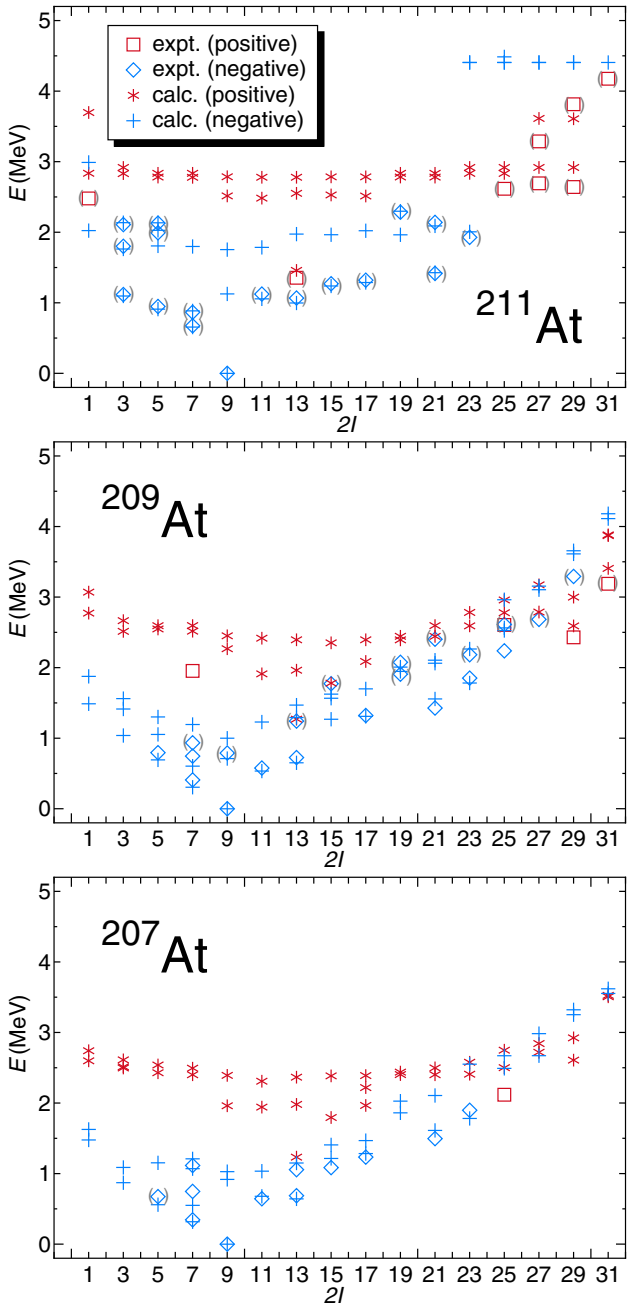

FIG. 7. Same as Fig. 1, but for odd-mass At isotopes. The experimental data are taken from Refs. [39,45,49,50].

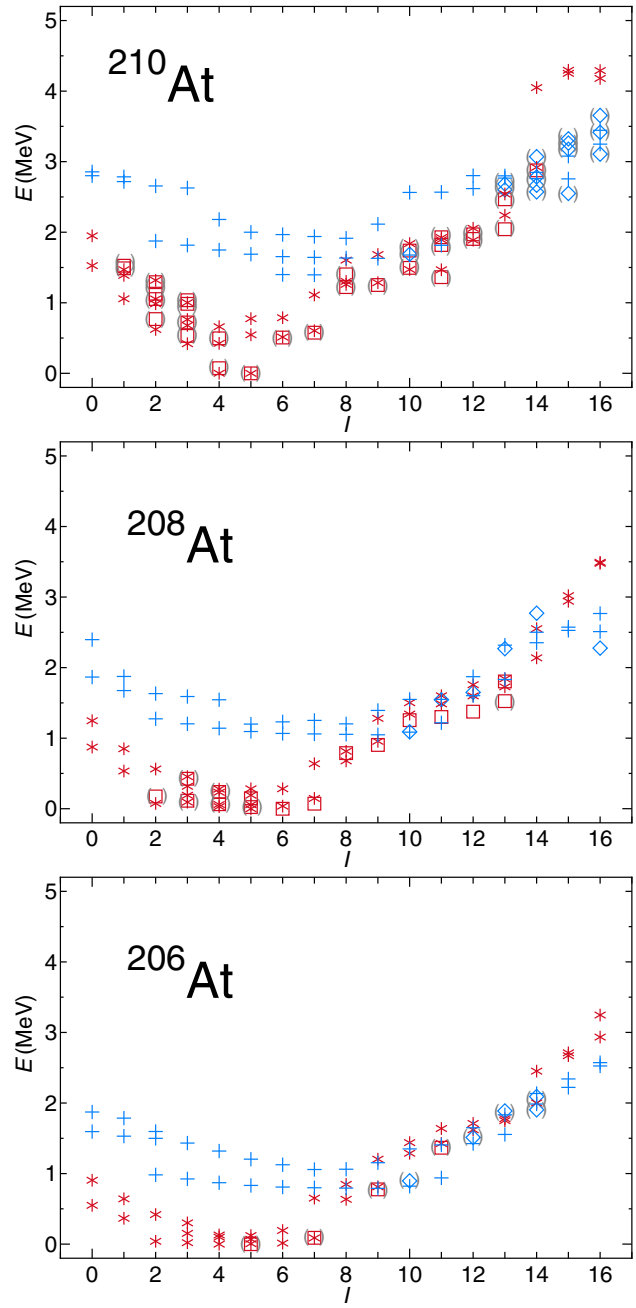

FIG. 8. Same as Fig. 1, but for doubly odd At isotopes. The experimental data are taken from Refs. [17,39,41,48].

the 14_1^+ state consists of the $(\pi h_{9/2}^3 f_{7/2})$ configuration. This difference of the configurations makes the $B(E2; 14_1^+ \rightarrow 12_1^+)$ value small. The 12_2^+ state consists of the $(\pi h_{9/2}^3 f_{7/2})$ configuration, and the $B(E2; 14_1^+ \rightarrow 12_2^+)$ value becomes large compared to the $B(E2; 14_1^+ \rightarrow 12_1^+)$ value. In ^{212}Rn, because of this small $B(E2)$ value, the 14_1^+ state is an isomer with a half-life of 7.4(8) ns [39]. Just like ^{212}Rn, the 14_1^+ state in ^{210}Rn (^{208}Rn) is an isomer with a half-life of 76(7) ns [3.5(7) ns] [39].

The experimental magnetic moments and quadrupole moments are well reproduced by the calculation. The largest difference between the experimental value and the theoretical one is seen in the quadrupole moment of the 17_1^- state for ^{210}Rn. The theoretical value is calculated 1.9 times lager than the experimental one.

F. Fr isotopes

Here $^{208-213}$Fr isotopes are discussed. Figure 11 shows the theoretical energy spectra for odd-mass Fr isotopes in comparison with the experimental data [39,49,50,53]. Negative parity yrast states are well reproduced in all the nuclei. Spin and parity of the ground state is $9/2^-$ for these odd-mass nuclei,

TABLE IX. Same as Table III, but for At isotopes. The experimental data are taken from Refs. [17,39,41,45,48–50].

^{211}At	Expt.	Calc.
$13/2^-_1 \to 9/2^-_1$	>0.039	4.298
$3/2^-_1 \to 5/2^-_1$	12.8(14)	9.801
$3/2^-_1 \to 7/2^-_1$	0.40(4)	0.874
$3/2^-_1 \to 7/2^-_2$	1.78(18)	0.828
$15/2^-_1 \to 11/2^-_1$	1.7(3)	2.271
$15/2^-_1 \to 13/2^-_1$	0.37(8)	0.598
$17/2^-_1 \to 13/2^-_1$	>84	4.108
$21/2^-_1 \to 17/2^-_1$	2.66(10)	2.119
$29/2^+_1 \to 25/2^+_1$	1.8(3)	1.054
^{209}At	Expt.	Calc.
$7/2^-_1 \to 9/2^-_1$		13.992
$11/2^-_1 \to 7/2^-_1$		3.226
$11/2^-_1 \to 9/2^-_1$		10.030
$21/2^-_1 \to 17/2^-_1$	3.21(10)	3.545
^{207}At	Expt.	Calc.
$7/2^-_1 \to 9/2^-_1$		17.889
$11/2^-_1 \to 7/2^-_1$		1.960
$11/2^-_1 \to 9/2^-_1$		13.164
^{210}At	Expt.	Calc.
$4^+_1 \to 5^+_1$		0.131
$6^+_1 \to 5^+_1$		3.226
$6^+_1 \to 4^+_1$		0.706
^{208}At	Expt.	Calc.
$5^+_1 \to 6^+_1$		2.129
$4^+_1 \to 6^+_1$		0.246
$4^+_1 \to 5^+_1$		2.913
^{206}At	Expt.	Calc.
$7^+_1 \to 5^+_1$		0.171
$9^+_1 \to 7^+_1$		13.618
$11^+_1 \to 9^+_1$		12.428

TABLE X. Same as Table VI, but for At isotopes. The experimental data are taken from Refs. [17,39,41,45,48–50].

^{211}At	μ		Q	
	Expt.	Calc.	Expt.	Calc.
$5/2^-_1$		+2.069		−0.007
$7/2^-_1$		+3.710		−0.475
$9/2^-_1$		+3.776		−0.211
$21/2^-_1$	+9.56(9)	+8.810	0.53(5)	−0.479
$29/2^+_1$	+15.31(13)	+14.129	1.00(5)	−1.092
^{209}At	Expt.	Calc.	Expt.	Calc.
$5/2^-_1$		+2.699		−0.014
$7/2^-_1$		+3.047		−0.776
$9/2^-_1$		+3.711		−0.372
$21/2^-_1$	+9.9(2)	+8.667	0.78(8)	−0.815
$29/2^+_1$	15.38(14)	+13.981	1.50(15)	−1.697
^{207}At	Expt.	Calc.	Expt.	Calc.
$5/2^-_1$		+2.629		−0.045
$7/2^-_1$		+3.011		−0.797
$9/2^-_1$		+3.680		−0.453
$25/2^+_1$	+3.75(13)	+2.870		+0.631
^{210}At	Expt.	Calc.	Expt.	Calc.
4^+_1		+3.543		−0.263
5^+_1		+3.980		−0.279
6^+_1		+4.107		−0.029
11^+_1	+9.79(3)	+8.832	0.65(8)	−0.610
19^+_1	13.26(13)	+12.746	2.20(25)	−0.810
15^-_1	+15.675(17)	+13.864	1.22(12)	−1.364
^{208}At	Expt.	Calc.	Expt.	Calc.
4^+_1		+3.027		−0.343
5^+_1		+3.456		−0.310
6^+_1		+3.889		−0.173
10^-_1	+2.69(3)	+2.318		+0.351
16^-_1		+13.971	1.7(3)	−1.839
^{206}At	Expt.	Calc.	Expt.	Calc.
5^+_1		+3.448		−0.322
7^+_1		+4.286		−0.309
9^+_1		+5.092		−0.254
11^+_1		+7.379		−0.446

which is reproduced in the calculation. Spin of the lowest positive parity states in these nuclei is 13/2, and energies of these states are calculated at 1.280, 1.101, and 1.166 MeV for ^{213}Fr, ^{211}Fr, and ^{209}Fr, respectively. These states mainly consist of the $[\pi(h_{9/2}f_{7/2})^4 i_{13/2}]$ configuration for the proton part.

The $29/2^+_1$ state in ^{213}Fr is a spin-gap isomer with a half-life of 238(6) ns [39]. This state decays to the $23/2^-_1$ state by the $E3$ transition. The $29/2^+_1$ state mainly consists of the $(\pi h^4_{9/2} i_{13/2})$ configuration, where two of four protons in the $0h_{9/2}$ orbital are coupled to spin eight and the rest two protons are coupled to spin zero. The last proton stays in the $0i_{13/2}$ orbital. The maximum spin of this configuration is 29/2. This isomer was also analyzed in Ref. [54] and they suggested the same configuration.

Figure 12 shows the theoretical energy spectra for doubly odd Fr isotopes in comparison with the experimental data [17,22,39,48,52]. There are a few observed states in these nuclei. In ^{208}Fr, spin and parity of the ground state is 7^+. However, the theoretical ground state becomes the 5^+, although the 2^+_1, 3^+_1, ..., 7^+_1 states are degenerately predicted around the ground state.

In ^{212}Fr, which is a system of one neutron and five protons, the lowest states are the 4^+ and 5^+ states. These two states consist of the $(\nu p^{-1}_{1/2} \pi h_{9/2})$ configuration coupled with the 0^+_1 state of the even-even core: ^{212}Rn. In contrast, in ^{208}Fr, which is a system of three neutrons and five protons, lowest states (2^+_1, 3^+_1, ..., 7^+_1) are members of the $(\nu f^{-1}_{5/2} \pi h_{9/2})$ configuration coupled with the 0^+_1 state of the even-even core: ^{208}Rn. It is seen from Fig. 12 that energies of negative parity states become lower and lower from ^{212}Fr to ^{208}Fr.

Calculated results of the $B(E2)$ values, magnetic moments and quadrupole moments for Fr isotopes are given in Tables XIII and XIV in comparison with the experimental data [17,39,48–50,52,53,55]. The small transition rates of the $B(E2; 17/2^-_1 \to 13/2^-_1)$ and $B(E2; 21/2^-_1 \to 17/2^-_1)$ values for ^{213}Fr are well reproduced. This nucleus is a system with five valence protons. All the $13/2^-_1$, $17/2^-_1$, and $21/2^-_1$ states

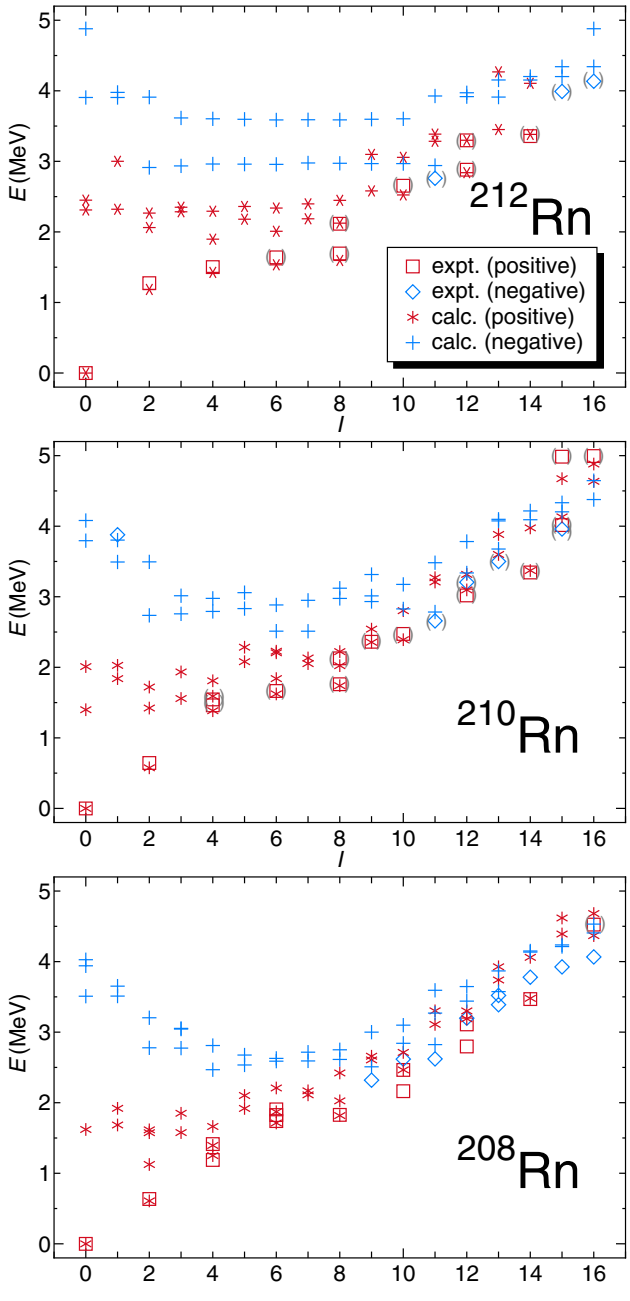

FIG. 9. Same as Fig. 1, but for even-even Rn isotopes. The experimental data are taken from Refs. [17,19,39,48,52].

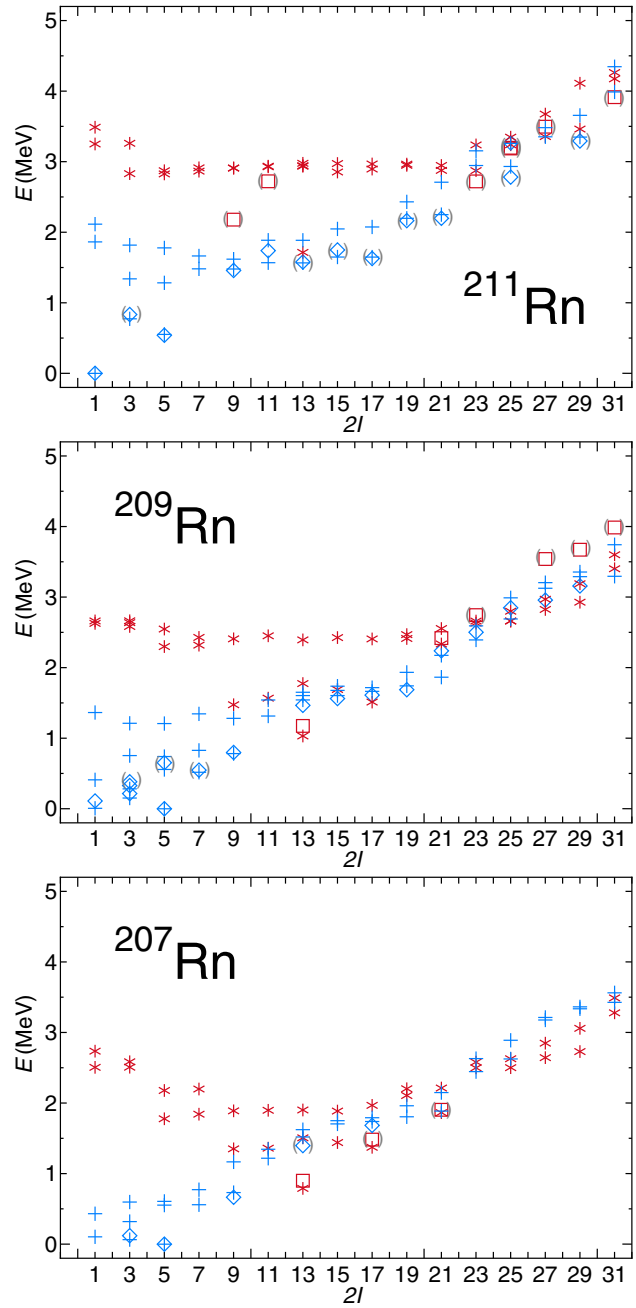

FIG. 10. Same as Fig. 1, but for odd-mass Rn isotopes. The experimental data are taken from Refs. [39,45,49,50].

are seniority $v = 3$ systems assuming the single-j ($j = h_{9/2}$) scheme. The $E2$ transition rates are hindered among states with the same seniority in this system [56]. Because of these small transition rates, the $17/2_1^-$ and $21/2_1^-$ states are isomers with half-lives of 505(14) ns and 18(1) ns [39]. It should be noted that the $9/2_1^-$ state has a seniority $v = 1$. Thus the $B(E2; 13/2_1^- \rightarrow 9/2_1^-)$ value is not hindered. Examples of these seniority isomers are also seen in the mass $A \sim 130$ region [16].

The quadrupole moments of the $9/2_1^-$ states for odd-mass nuclei are calculated several times smaller than experimental values. However, the magnetic moments of the same states are well reproduced.

IV. DISCUSSION

A. Magnetic moments and quadrupole moments

As discussed in Sec. III B, the following observations are found in various cases; the calculated quadrupole moment of one specific state does not agree with the experimental data even though the calculated magnetic moment of the same state agrees with the experimental data. This phenomenon was also

TABLE XI. Same as Table III, but for Rn isotopes. The experimental data are taken from Refs. [17,39,45,48–50,52].

^{212}Rn	Expt.	Calc.
$2_1^+ \to 0_1^+$		6.237
$4_1^+ \to 2_1^+$	1.04(4)	0.688
$6_1^+ \to 4_1^+$	0.40(5)	0.373
$8_1^+ \to 6_1^+$	0.115(6)	0.144
$10_1^+ \to 8_1^+$		3.950
$12_1^+ \to 10_1^+$	4.4(2)	2.966
$14_1^+ \to 12_1^+$	0.032(8)	0.0024
$14_1^+ \to 12_2^+$	<4	2.856
$17_1^- \to 15_1^-$	3.0(16)	2.111
^{210}Rn	Expt.	Calc.
$2_1^+ \to 0_1^+$		12.230
$4_1^+ \to 2_1^+$		18.353
$6_1^+ \to 4_1^+$	1.58(15)	1.337
$6_1^+ \to 4_2^+$	1.58(19)	2.631
$8_1^+ \to 6_1^+$		0.704
$14_1^+ \to 12_1^+$	0.0248(23)	0.001
^{208}Rn	Expt.	Calc.
$2_1^+ \to 0_1^+$		19.125
$4_1^+ \to 2_1^+$		10.300
$6_1^+ \to 4_1^+$		0.329
$8_1^+ \to 6_1^+$		1.417
^{211}Rn	Expt.	Calc.
$5/2_1^- \to 1/2_1^-$	>0.040	5.024
$3/2_1^- \to 1/2_1^-$		7.002
$3/2_1^- \to 5/2_1^-$		1.484
$21/2_1^- \to 17/2_1^-$	>0.030	4.867
$25/2_1^- \to 21/2_1^-$	>0.036	2.627
$29/2_1^- \to 25/2_1^-$	0.073(17)	0.001
$29/2_1^- \to 25/2_2^-$	1.9(6)	1.567
$31/2_1^+ \to 27/2_1^+$	>0.0077	3.340
^{209}Rn	Expt.	Calc.
$1/2_1^- \to 5/2_1^-$		1.210
$3/2_1^- \to 5/2_1^-$		6.837
$3/2_1^- \to 1/2_1^-$		0.071
$29/2_1^- \to 27/2_1^-$	0.66 (15)	0.107
^{207}Rn	Expt.	Calc.
$3/2_1^- \to 5/2_1^-$		5.024
$9/2_1^- \to 5/2_1^-$		17.633
$17/2_1^- \to 13/2_1^-$		4.179
$17/2_1^+ \to 13/2_1^+$		17.878
$21/2_1^+ \to 17/2_1^+$		4.860

TABLE XII. Same as Table VI, but for Rn isotopes. The experimental data are taken from Refs. [17,39,45,48–50,52].

^{212}Rn	μ		Q	
	Expt.	Calc.	Expt.	Calc.
2_1^+		+1.714		+0.002
4_1^+	4.0(2)	+3.369		+0.040
6_1^+	5.45(5)	+5.058		−0.020
8_1^+	+7.15(2)	+6.726		−0.193
14_1^+	15.0(4)	+13.207		−0.881
17_1^-	17.9(2)	+16.205		−1.021
^{210}Rn	Expt.	Calc.	Expt.	Calc.
2_1^+		+0.470		+0.508
4_1^+		+1.603		+0.504
6_1^+		+4.937		−0.043
8_1^+	7.184(56)	+6.611	0.31(4)	−0.300
14_1^+	14.92(10)	+13.060		−1.402
11_1^-	12.16(11)	+11.014		−1.343
17_1^-	17.88(9)	+16.088	0.86(10)	−1.655
^{208}Rn	Expt.	Calc.	Expt.	Calc.
2_1^+		+0.604		+0.107
4_1^+		+0.569		+0.948
6_1^+		+4.908		−0.118
8_1^+	6.98(8)	+6.529	0.39(5)	−0.426
10_1^-	10.77(10)	+10.136		−1.843
^{211}Rn	Expt.	Calc.	Expt.	Calc.
$1/2_1^-$	+0.601(7)	+0.315		
$3/2_1^-$		−0.451		+0.229
$5/2_1^-$		+0.903		+0.373
$17/2_1^-$	+7.75(8)	+6.940	0.18(2)	−0.240
$13/2_1^+$		−0.919		+0.675
^{209}Rn	Expt.	Calc.	Expt.	Calc.
$1/2_1^-$		+0.317		
$3/2_1^-$		−0.513		+0.154
$5/2_1^-$	0.8388(4)	+0.661	+0.31(3)	+0.458
$13/2_1^+$		−0.915		+0.831
^{207}Rn	Expt.	Calc.	Expt.	Calc.
$1/2_1^-$		+0.309		
$3/2_1^-$		−0.553		+0.367
$5/2_1^-$	+0.816(9)	+0.638	+0.220(22)	+0.285
$13/2_1^+$	−0.903(3)	−0.917		+0.815

frequently seen in nuclei around mass 130 [16]. Here we try to shed light on this issue.

This phenomenon might be explained by the sensitiveness of operators on the mixture of states. Our assertion is made as follows. If the true state is a mixture of one main state and another secondary state, the quadrupole moment is largely affected by this admixture whereas the the magnetic moment is less affected.

Suppose that two states with the same spin and parity are slightly mixed,

$$|\varphi\rangle = \alpha|\varphi_1\rangle + \sqrt{1-\alpha^2}|\varphi_2\rangle, \tag{12}$$

where $|\varphi_1\rangle$ and $|\varphi_2\rangle$ represent the main state and the secondary one, respectively. Here it is assumed that the mixing amplitude α is real and $|\alpha| \simeq 1$. Then any electromagnetic moment is approximately calculated as

$$\langle\varphi|\hat{O}|\varphi\rangle \sim \alpha^2\langle\varphi_1|\hat{O}|\varphi_1\rangle + 2\alpha\sqrt{1-\alpha^2}\langle\varphi_1|\hat{O}|\varphi_2\rangle, \tag{13}$$

where $\hat{O}$ is either the magnetic moment operator or the quadrupole moment operator. To see influences by the admixture of the first (main) and the second (secondary) states, the mixing ratios of two states for the operator $\hat{O}$ defined by $S = \langle\varphi_1|\hat{O}|\varphi_2\rangle/\langle\varphi_1|\hat{O}|\varphi_1\rangle$ are numerically evaluated for the magnetic moment and the quadrupole moment.

For the 10_1^- state of ^{206}Bi, it is calculated as $S_M = -0.147$ for the magnetic moment and as $S_Q = -1.295$ for the quadrupole moment. Here $|\varphi_1\rangle = |10_1^-\rangle$ and $|\varphi_2\rangle = |10_2^-\rangle$

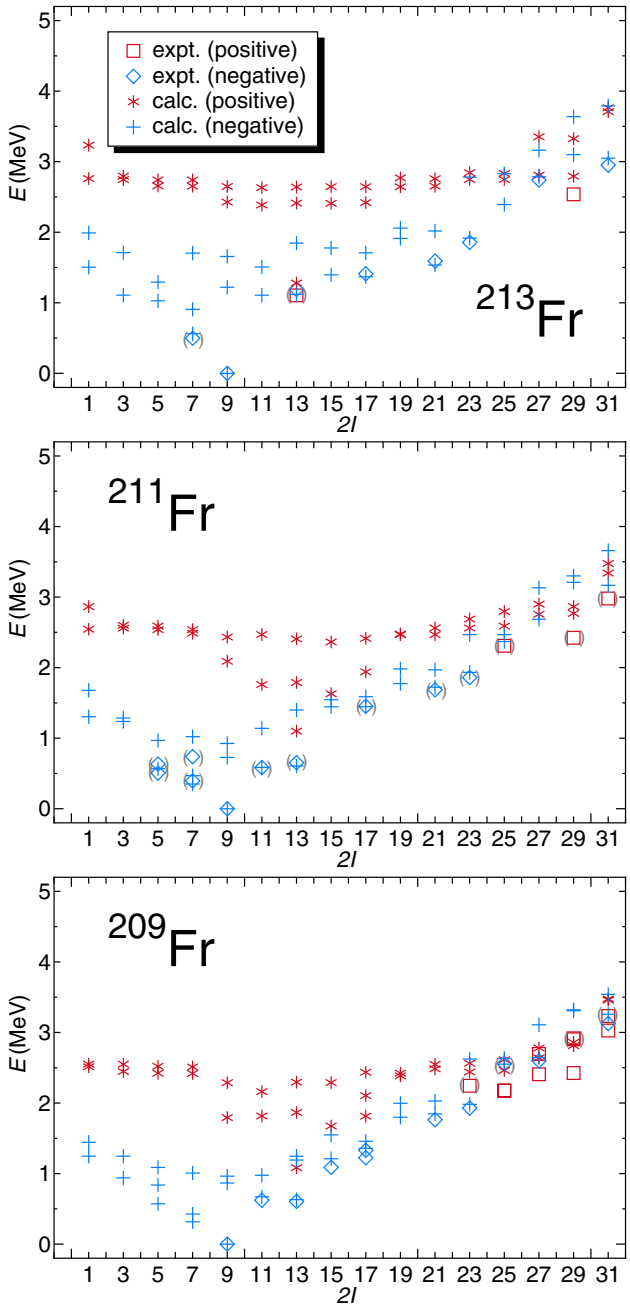

FIG. 11. Same as Fig. 1, but for odd-mass Fr isotopes. The experimental data are taken from Refs. [39,49,50,53].

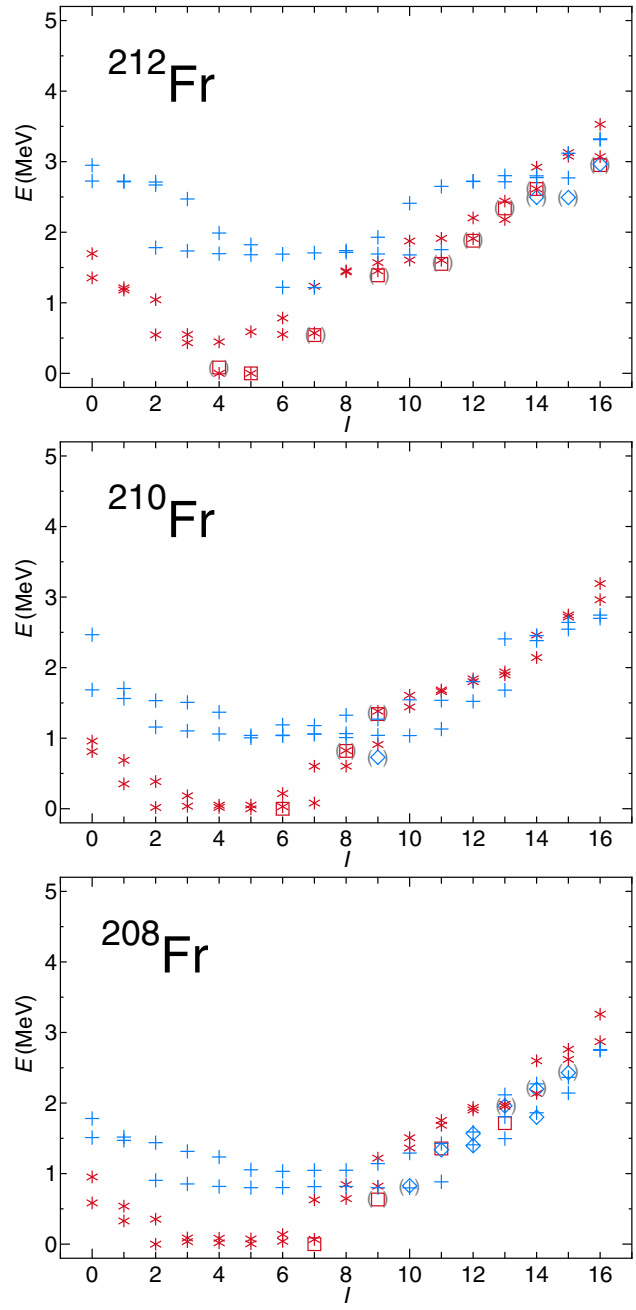

FIG. 12. Same as Fig. 1, but for doubly odd Fr isotopes. The experimental data are taken from Refs. [17,22,39,48,52].

are assumed. For the 10_1^- state of ^{204}Bi, it is calculated as $S_M = -0.123$ for the magnetic moment and as $S_Q = -0.719$ for the quadrupole moment. It is generally true that the S values of the quadrupole moments are at least several times larger than those of the magnetic moments. Namely, the quadrupole moment is more sensitive to the admixture of states than the magnetic moment.

To see the actual effect of admixture of two neighboring states, magnetic moments and quadrupole moments are calculated with and without admixture of states assuming appropriate mixing amplitude α's. Table XV shows calculated magnetic moments and quadrupole moments in comparison with those by the admixture of states for the 10_1^- states of ^{206}Bi and ^{204}Bi in comparison with the experimental data. $\alpha = 0.979$ (0.940) is taken for ^{206}Bi (^{204}Bi), which is so determined that each ratio of the calculated quadrupole moment after mixing to the experimental one becomes two. Then the ratio of the calculated magnetic moment to the experimental one is reduced from 0.85 to 0.76 for ^{206}Bi. Thus the calculated magnetic moment is slightly deteriorated whereas the quadrupole moment is largely improved. ^{204}Bi also shows a similar tendency. This analysis also shows that admixture of neighboring states is insufficient

TABLE XIII. Same as Table III, but for Fr isotopes. The experimental data are taken from Refs. [17,39,48–50,52,53,55].

^{213}Fr	Expt.	Calc.
$7/2^-_1 \to 9/2^-_1$		1.056
$13/2^-_1 \to 9/2^-_1$	>0.0015	5.770
$17/2^-_1 \to 13/2^-_1$	0.55(4)	0.010
$21/2^-_1 \to 17/2^-_1$	0.0439(20)	0.071
$27/2^-_1 \to 23/2^-_1$	0.001960(4)	4.061
$31/2^-_1 \to 27/2^-_1$	1.133(14)	3.260
^{211}Fr	Expt.	Calc.
$7/2^-_1 \to 9/2^-_1$		15.564
$5/2^-_1 \to 7/2^-_1$		3.156
$5/2^-_1 \to 9/2^-_1$		11.866
$13/2^-_1 \to 9/2^-_1$	>0.063	12.832
$17/2^-_1 \to 13/2^-_1$	>0.011	17.934
$21/2^-_1 \to 17/2^-_1$	3.9(4)	3.520
$29/2^+_1 \to 25/2^+_1$	0.38(8)	0.376
^{209}Fr	Expt.	Calc.
$13/2^-_1 \to 9/2^-_1$		19.673
$11/2^-_1 \to 9/2^-_1$		17.628
$23/2^-_1 \to 21/2^-_1$	>1.6	0.478
^{212}Fr	Expt.	Calc.
$4^+_1 \to 5^+_1$		0.002
$7^+_1 \to 5^+_1$		5.369
$11^+_1 \to 9^+_1$	0.00095(3)	0.194
^{210}Fr	Expt.	Calc.
$8^+_1 \to 6^+_1$		5.586
$9^+_1 \to 8^+_1$		0.816
^{208}Fr	Expt.	Calc.
$9^+_1 \to 7^+_1$		18.092

to simultaneously explain disagreements with experiment for the quadrupole moment and the magnetic moment. This phenomenon should be further investigated in a future study.

The reason for different sensitivities to the admixture of states for the quadrupole moment and the magnetic moment might be surmised as follows. The magnetic moment operator as a one-body operator changes spin up to only one. In contrast the quadrupole moment one-body operator changes spin up to two. It is inferred that the quadrupole moment operator more largely mixes single-particle orbitals compared to the magnetic moment operator and consequently the quadrupole moment is more easily affected by the admixture of states.

B. MP-8 interaction

In this study, a specific interaction with spin 8 between protons in the $0h_{9/2}$ and $1f_{7/2}$ orbitals (MP-8) given in Eq. (7) was added as part of an effective interaction. In this section the necessity of this interaction is discussed.

Figure 13 shows the theoretical energy spectra for positive parity states in ^{210}Po with and without the MP-8 interaction in comparison with the experimental data [39,48]. The theoretical calculation well reproduces the experimental data with the MP-8 interaction. By comparing results with and without the MP-8 interaction, it is concluded that the influences coming from the MP-8 interaction are not so large on almost all the

TABLE XIV. Same as Table VI, but for Fr isotopes. The experimental data are taken from Refs. [17,39,48–50,52,53].

^{213}Fr	μ		Q	
	Expt.	Calc.	Expt.	Calc.
$7/2^-_1$		+4.187		−0.283
$9/2^-_1$	+4.02(8)	+3.780	−0.14(2)	−0.024
$17/2^-_1$	7.5(14)	+7.164		−0.022
$21/2^-_1$	9.32(3)	+8.819		−0.032
$13/2^+_1$		+7.394		−0.440
$29/2^+_1$	15.22(3)	+14.120		−0.709
^{211}Fr	Expt.	Calc.	Expt.	Calc.
$7/2^-_1$		+3.332		−0.463
$9/2^-_1$	+4.00(8)	+3.726	−0.19(3)	−0.048
$13/2^+_1$		+7.277		−1.192
$29/2^+_1$	15.37(15)	+13.936	−1.1(2)	−1.166
^{209}Fr	Expt.	Calc.	Expt.	Calc.
$7/2^-_1$		+3.363		−0.482
$9/2^-_1$	+3.95(2)	+3.692	−0.24(2)	−0.129
$13/2^+_1$		+7.261		−1.381
^{212}Fr	Expt.	Calc.	Expt.	Calc.
4^+_1		+3.419		−0.028
5^+_1	4.62(9)	+4.079	−0.10(1)	−0.032
7^+_1		+4.678		+0.255
11^+_1	9.89(4)	+9.096		−0.022
22^+_1	22(4)	+14.954		−0.470
15^-_1	15.64(12)	+14.030	0.84(13)	−0.906
^{210}Fr	Expt.	Calc.	Expt.	Calc.
6^+_1	+4.40(9)	+3.948	+0.19(2)	+0.291
8^+_1		+4.638		+0.183
9^+_1		+4.940		+0.487
^{208}Fr	Expt.	Calc.	Expt.	Calc.
7^+_1	4.75(10)	+4.318	0.00(4)	+0.050
9^+_1		+4.927		+0.014
10^-_1		+2.314		+0.726

TABLE XV. Magnetic moments and quadrupole moments with and without mixing of the second excited states for 10^-_1 states of Bi isotopes in comparison with the experimental data. Calc1 (Ratio1) represents the initial magnetic and quadrupole moments (ratio of the initial moment to the experimental value) without admixture of states. Calc2 (Ratio2) represents magnetic and quadrupole moments (ratio of the calculated moment after mixing to the experimental value) with admixture of the second excited states. The mixing amplitude $\alpha = 0.979$ is taken for ^{206}Bi and $\alpha = 0.940$ is taken for ^{204}B.

^{206}Bi (10^-_1)	Expt.	Calc1	Calc2	Ratio1	Ratio2
Q	0.049(9)	−0.225	−0.098	4.59	**2.00**
μ	2.644(14)	+2.259	+2.030	0.85	0.76
^{204}Bi (10^-_1)	Expt.	calc1	calc2	ratio1	ratio2
Q	0.063(12)	−0.298	−0.126	4.74	**2.00**
μ	2.36(23)	+2.269	+1.827	0.96	0.77

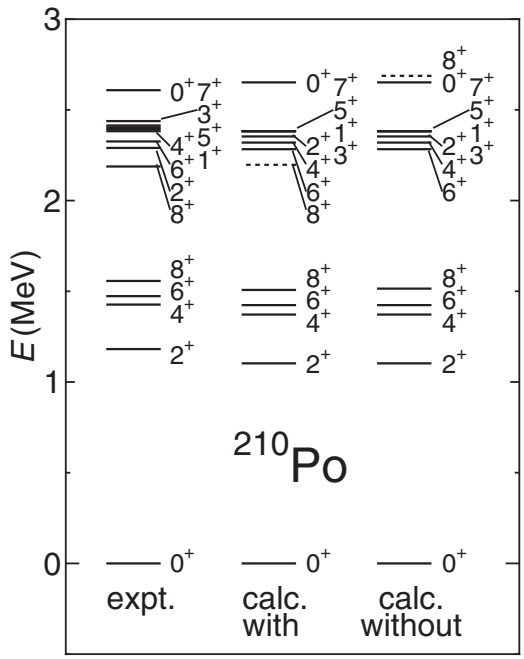

FIG. 13. Comparison between the experimental spectra (expt.) and the shell-model results with (calc. with) and without (calc. without) the MP-8 interaction for positive parity states in ^{210}Po. The experimental data are taken from Refs. [39,48]. The states with the energy difference of more than 0.1 MeV between those with and without the MP-8 interaction are indicated by dotted lines.

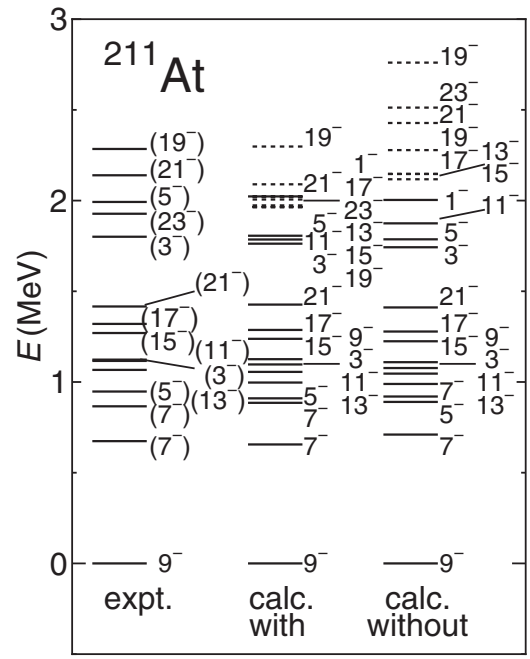

FIG. 14. Same as Fig. 13, but for negative parity states of ^{211}At. Spin is denoted by twice the original value. The experimental data are taken from Refs. [39,50]. Only the first and second states for each spin are shown.

states except for the 8_2^+ state. The calculated energy of the 8_2^+ state without the MP-8 interaction is 0.490 MeV higher than that with the MP-8 interaction. The 8_1^+ state mainly consists of the $(\pi h_{9/2}^2)$ configuration whereas the 8_2^+ state mainly consists of the $(\pi h_{9/2} f_{7/2})$ configuration. Therefore the 8_2^+ state is directly affected by the MP-8 interaction.

Figure 14 shows the theoretical energy spectra for negative parity states in ^{211}At with and without the MP-8 interaction in comparison with the experimental data [39,50]. Low-lying states below 1.5 MeV are not at all affected by the MP-8 interaction. However, large influences are seen for energy levels over 1.5 MeV. For example, the $23/2_1^-$ state is not well reproduced without the MP-8 interaction. Because the $23/2_1^-$ state is found to consist of the $[\pi h_{9/2}(h_{9/2} f_{7/2})^2_{8^+}]$ configuration, the state is largely affected by the MP-8 interaction.

Figure 15 shows the theoretical energy spectra for positive parity states in ^{212}Rn with and without the MP-8 interaction in comparison with the experimental data [39,52]. There are no influences on the low-lying states below 1.5 MeV. However, the 8_2^+, 12_2^+, and 14_1^+ states are not well reproduced without the MP-8 interaction. This is because of the fact that the 8_2^+, 12_2^+, and 14_1^+ states mainly consist of the $[\pi(h_{9/2}^2)_{I^+}(h_{9/2} f_{7/2})_{8^+}]$ configuration, where those states with $I = 0$, $I = 4$, and $I = 6$ correspond to the 8_2^+, 12_2^+, and 14_1^+ states, respectively.

As a phenomenological study any kind of two-body interactions which act on nucleons in any two orbitals should be introduced for a better fit to the experimental data, but only the MP-8 interaction is introduced in the present study. This is because both the $0h_{9/2}$ and $1f_{7/2}$ orbitals are the most low-lying orbitals for protons and influences from these two low-lying orbitals are dominantly observed in experiment. However, why spin of this specific interaction must be eight,

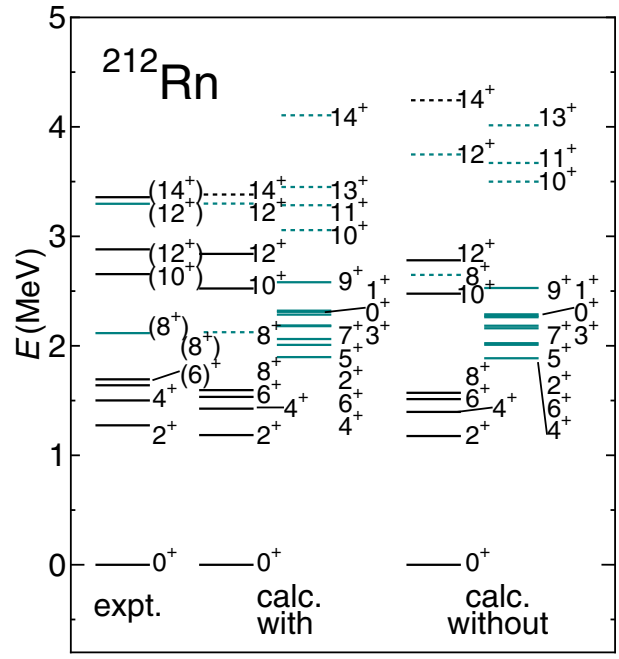

FIG. 15. Same as Fig. 13, but for positive parity states of ^{212}Rn. The experimental data are taken from Refs. [39,52]. Only the first and second states for each spin are shown. The 14_2^+ state calculated without the MP-8 interaction is not shown in the figure, but this state is predicted at 5.282 MeV.

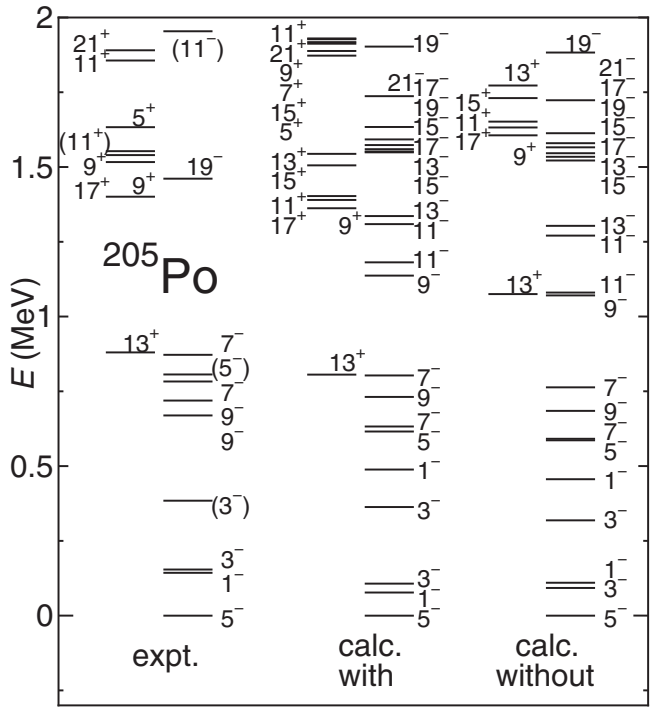

FIG. 16. Comparison between the experimental spectra (expt.) and the shell-model results with (calc. with) and without (calc. without) the particle number dependence of the $i_{13/2}$ orbitals for ^{205}Po. The experimental data are taken from Refs. [39,43]. Only the first and second states for each spin and parity are shown. Spin is denoted by twice the original value.

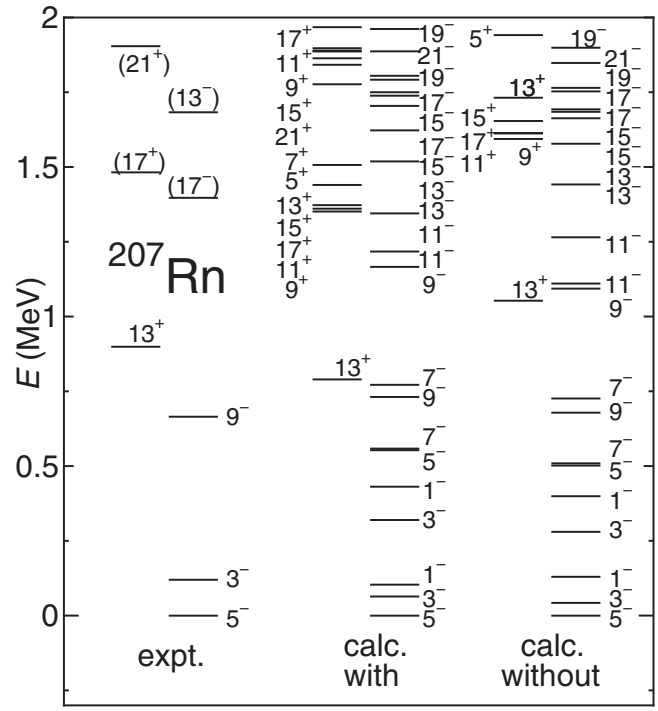

FIG. 17. Same as Fig. 16, but for ^{207}Rn. The experimental data are taken from Refs. [39,45].

is not clarified from the present analysis. The reason might be related to the fact that spin 8 is the maximum spin in both the $(\pi h_{9/2}^2)$ and $(\pi h_{9/2} f_{7/2})$ configurations. The detailed analysis, however, is necessary in a future analysis.

C. The particle number dependence of the $i_{13/2}$ orbitals

In this study, it was assumed that single-particle energies of the neutron and the proton $0i_{13/2}$ orbitals change linearly with the numbers of valence neutron holes and proton particles. These number dependencies are introduced for better descriptions of energies of the $13/2_1^+$ states of odd-mass nuclei. It should be noted, however, that the influences of these number dependencies are not large and rough energies of the $13/2_1^+$ states are reproduced without the number dependencies.

Figures 16 and 17 show the theoretical energy spectra for positive parity states in ^{205}Po and ^{207}Rn with and without the number dependence of the $0i_{13/2}$ orbitals in comparison with the experimental data [39,43,45]. For calculations without the number dependencies, single-particle energies of the $0i_{13/2}$ orbitals are taken as 1.633 MeV for neutrons and 1.609 MeV for protons, which are taken from the experimental excitation energies of ^{207}Pb (for neutrons) and ^{209}Bi (for protons). With the number dependencies, energies of positive parity states are better reproduced than those without the number dependencies, but differences of these two results are small.

It is known that the single-particle energies are shifted by the effects of the monopole interactions of the nucleon-nucleon (NN) interaction as protons or neutrons occupy certain orbitals [57–59]. There are a lot of studies which consider the effects of the monopole interaction in lighter mass regions (e.g., see Ref. [60]). For example, a mechanism of change of single-particle energies in the p- and sd-shell regions were studied by analyzing contributions from different components of NN interactions [61]. It was shown that the neutron-proton monopole interactions play an important role for the change of the single-particle energies and the triplet-even component from the central interactions and the second-order tensor correlations are dominant for the monopole interaction.

Because the present study is carried out from a phenomenological point of view, the shifts of single-particle energies coming from the monopole interactions are not considered. The number dependence of the single-particle energy was introduced only for the $0i_{13/2}$ orbitals. It is because this effect is easily seen because parity of the $0i_{13/2}$ orbital is only positive among all the orbitals. As a phenomenological study we do not pursue this number-dependence problem of single-particle energies any further, but this issue is so important that it should be studied in the future from the point of view of the monopole interactions.

D. The $\nu i_{13/2}^{-1} \otimes \pi i_{13/2}$ band

In the medium and heavy nuclei, intruder orbitals are important to describe the low-lying nuclear structure. For example, the intruder orbital between the magic numbers 28 and 50 is the $0g_{9/2}$ orbital and this orbital plays an important role for the nuclear structure. In the region between the

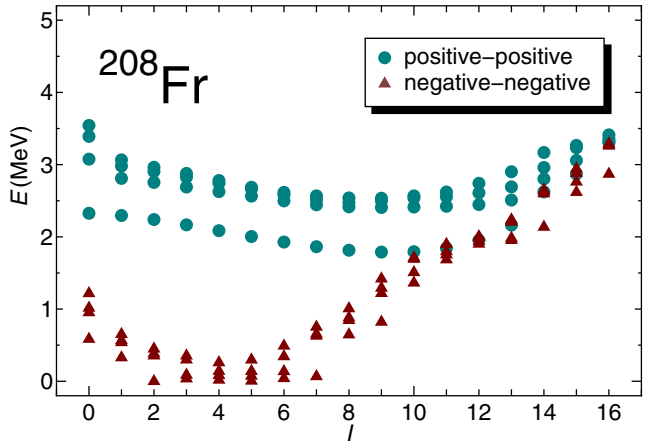

FIG. 18. Theoretical energy levels for positive parity states in ^{208}Fr. The circles and triangles represent the theoretical results of the positive-positive configuration and negative-negative configurations, respectively. Up to four calculated states are shown for each spin and each configuration.

magic numbers 50 and 82, the intruder orbital is the $0h_{11/2}$ orbital and states with the $(\nu h_{11/2}^{-1}\pi h_{11/2})$ configuration are observed and analyzed in doubly odd nuclei in the mass $A \sim 130$ region (e.g., see references in Ref. [62]). In the mass $A \sim 130$ region, states which have the $(\nu h_{11/2}^{-1}\pi h_{11/2})$ configuration are occasionally located below those states with the positive-positive configuration, where the positive-positive configuration means that the state consists of a positive-parity state for the neutron part and also a positive-parity state for the proton part. Note that only the $0h_{11/2}$ orbital has negative parity and other orbitals have positive parity in the mass $A \sim 130$ region. The yrast and yrare bands with the $(\nu h_{11/2}^{-1}\pi h_{11/2})$ configuration are experimentally found to be almost degenerate in energy. These bands are called $\Delta I = 1$ doublet bands [63–65].

In the region treated in this study, the intruder orbital is the $0i_{13/2}$ orbital. Only this orbital has positive parity among the six orbitals in this region. Just like the nuclei in the mass $A \sim 130$ region, states with the $(\nu i_{13/2}^{-1}\pi i_{13/2})$ configuration are expected to be observed in doubly odd nuclei.

Figure 18 shows the calculated energy levels of the positive parity states for ^{208}Fr, which are separately shown for the positive-positive configuration and the negative-negative configurations. Here states of the positive-positive configuration mean those states which consist of the positive-parity state for the neutron part and the positive-parity state for the proton part. Namely these states have the $(\nu i_{13/2}^{-1}\pi i_{13/2})$ configuration. States of the negative-negative configuration means those states which consist of the negative-parity state for the neutron part and the negative-parity state for the proton part.

As seen in Fig. 18 states of the positive-positive configuration are calculated over 2.0 MeV. It is theoretically found that the lowest $0^+, 1^+, \ldots, 13^+$ states with the positive-positive configuration located at $2.0 \sim 2.5$ MeV, consist of the $(\nu i_{13/2}^{-1}\pi i_{13/2})$ configuration coupled with the 0_1^+ state of the corresponding even-even core of ^{208}Rn. States over these states with the positive-positive configuration consist of the $(\nu i_{13/2}^{-1}\pi i_{13/2})$ configuration coupled with the $2_1^+, 4_1^+, \ldots$ states of the ^{208}Rn core. In ^{208}Fr, states with the $(\nu i_{13/2}^{-1}\pi i_{13/2})$ configuration are calculated in energy above the negative-negative configuration in low-spin states. Thus no $\Delta I = 1$ doublet bands are expected in this region at least near ^{208}Pb as the yrast band.

In the mass $A \sim 130$ region, the neutron $0h_{11/2}$ orbital is one of the low-lying orbital and the proton $0h_{11/2}$ orbital is located about 2.8 MeV from a doubly magic core. In contrast, the $0i_{13/2}$ orbitals are located in the middle of the shell for neutrons and protons in the mass $A \sim 210$ region. To make the $(\nu i_{13/2}^{-1}\pi i_{13/2})$ configuration, both one neutron and one proton need to be excited to the $0i_{13/2}$ orbitals. For the calculation of ^{208}Fr, the $0i_{13/2}$ orbital for neutrons is located at 1.373 MeV and the $0i_{13/2}$ orbital for protons is located at 1.409 MeV in our calculation. In much lighter Fr isotopes one may find those states with the $(\nu i_{13/2}^{-1}\pi i_{13/2})$ configuration as the yrast states.

V. SUMMARY

In the present study, the large-scale shell-model calculations have been carried out for even-even, odd-mass, and doubly odd nuclei of Pb, Bi, Po, At, Rn, and Fr isotopes in the neutron deficit region around the ^{208}Pb nucleus.

As for single-particle orbitals, all the six orbitals between the magic numbers 82 and 126 ($0h_{9/2}$, $1f_{7/2}$, $0i_{13/2}$, $2p_{3/2}$, $1f_{5/2}$, and $2p_{1/2}$) have been taken. The particle number dependence on the $0i_{13/2}$ single-particle energies was assumed. They are changed linearly so as to reproduce energy levels of the low-lying positive parity states. As for the effective two-body interaction, higher multipole-paring interactions are employed for identical nucleons and the quadrupole-quadrupole interaction between neutrons and protons. Only one set of the strengths was assumed in all the nuclei considered. The additional interaction with spin 8 (MP-8) was introduced between the proton $0h_{9/2}$ and $0f_{7/2}$ orbitals for the proton part as shown in Eq. (7). The effects of this interaction have been discussed.

The energy spectra, $E2$ transition rates, magnetic moments, and quadrupole moments have been calculated and compared with the experimental data. Good agreements with the experimental data have been obtained not only for even-even and odd-mass nuclei, but also for doubly odd nuclei. Energy levels in this mass region are much better reproduced than those in lighter mass regions like mass 80 [7] and 130 [16] regions.

ACKNOWLEDGMENTS

This work was supported by Grant-in-Aid for Scientific Research (C) (Grants No. 24540251 and No. 25400267) from Japan Society for the Promotion of Science (JSPS) and also by a Grant-in-Aid for JSPS Fellows (Grant No. 26.10429).

[1] G. H. Lang, C. W. Johnson, S. E. Koonin, and W. E. Ormand, Phys. Rev. C **48**, 1518 (1993).
[2] M. Honma, T. Mizusaki, and T. Otsuka, Phys. Rev. Lett. **75**, 1284 (1995).
[3] N. Yoshinaga and A. Arima, Phys. Rev. C **81**, 044316 (2010).
[4] M. Honma, T. Otsuka, B. A. Brown, and T. Mizusaki, Phys. Rev. C **69**, 034335 (2004).
[5] D. Rudolph, C. Baktash, M. J. Brinkman, M. Devlin, H.-Q. Jin, D. R. LaFosse, L. L. R. and D. G. Sarantites, and C.-H. Yu, Eur. Phys. J. A **4**, 115 (1999).
[6] B. Cheal, E. Mané, J. Billowes, M. L. Bissell, K. Blaum, B. A. Brown, F. C. Charlwood, K. T. Flanagan, D. H. Forest, C. Geppert, M. Honma, A. Jokinen, M. Kowalska, A. Krieger, J. Krämer, I. D. Moore, R. Neugart, G. Neyens, W. Nörtershäuser, M. Schug, H. H. Stroke, P. Vingerhoets, D. T. Yordanov, and M. Žáková, Phys. Rev. Lett. **104**, 252502 (2010).
[7] N. Yoshinaga, K. Higashiyama, and P. H. Regan, Phys. Rev. C **78**, 044320 (2008).
[8] M. Honma, T. Otsuka, T. Mizusaki, and M. Hjorth-Jensen, Phys. Rev. C **80**, 064323 (2009).
[9] K. Sieja, F. Nowacki, K. Langanke, and G. Martínez-Pinedo, Phys. Rev. C **79**, 064310 (2009).
[10] K. Higashiyama, N. Yoshinaga, and K. Tanabe, Phys. Rev. C **65**, 054317 (2002).
[11] L. Coraggio, A. Covello, A. Gargano, N. Itaco, and T. T. S. Kuo, Phys. Rev. C **66**, 064311 (2002).
[12] A. Gargano, Eur. Phys. J. A **20**, 103 (2004).
[13] H. Jin, M. Hasegawa, S. Tazaki, K. Kaneko, and Y. Sun, Phys. Rev. C **84**, 044324 (2011).
[14] A. Astier, M.-G. Porquet, T. Venkova, D. Verney, C. Theisen, G. Duchêne, F. Azaiez, G. Barreau, D. Curien, I. Deloncle, O. Dorvaux, B. J. P. Gall, M. Houry, R. Lucas, N. Redon, M. Rousseau, and O. Stézowski, Phys. Rev. C **85**, 064316 (2012).
[15] H.-K. Wang, Y. Sun, H. Jin, K. Kaneko, and S. Tazaki, Phys. Rev. C **88**, 054310 (2013).
[16] E. Teruya, N. Yoshinaga, K. Higashiyama, and A. Odahara, Phys. Rev. C **92**, 034320 (2015).
[17] M. J. Martin, Nucl. Data Sheets **108**, 1583 (2007).
[18] S. Bayer, A. P. Byrne, G. D. Dracoulis, A. M. Baxter, T. Kibedi, and F. G. Kondev, Nucl. Phys. A **694**, 3 (2001).
[19] J. J. Ressler, C. W. Beausang, H. Ai, H. Amro, M. A. Caprio, R. F. Casten, A. A. Hecht, S. D. Langdown, E. A. McCutchan, D. A. Meyer, P. H. Regan, M. J. S. Sciacchitano, A. Yamamoto, and N. V. Zamfir, Phys. Rev. C **69**, 034331 (2004).
[20] F. Hessberger, S. Hofmann, I. Kojouharov, and D. Ackermann, Eur. Phys. J. A **22**, 253 (2004).
[21] G. D. Dracoulis, G. J. Lane, A. P. Byrne, P. M. Davidson, T. Kibédi, P. Nieminen, K. H. Maier, H. Watanabe, and A. N. Wilson, Phys. Rev. C **77**, 034308 (2008).
[22] G. D. Dracoulis, P. M. Davidson, G. J. Lane, A. P. Byrne, T. Kibédi, P. Nieminen, A. N. Wilson, and H. Watanabe, Eur. Phys. J. A **40**, 127 (2009).
[23] N. Cieplicka, K. H. Maier, B. Fornal, B. Szpak, R. V. F. Janssens, M. Alcorta, R. Broda, M. P. Carpenter, C. J. Chiara, C. R. Hoffman, B. P. Kay, F. G. Kondev, W. Królas, T. Lauritsen, C. J. Lister, E. A. McCutchan, T. Pawlat, A. M. Rogers, D. Seweryniak, N. Sharp, W. B. Walters, J. Wrzesiński, and S. Zhu, Phys. Rev. C **86**, 054322 (2012).
[24] C. Fry and M. Thoennessen, Atomic Data and Nuclear Data Tables **99**, 365 (2013).
[25] C. Fry and M. Thoennessen, Atomic Data and Nuclear Data Tables **99**, 497 (2013).
[26] K. H. Maier, D. J. Decman, H. Grawe, H. Haas, and W.-D. Zeitz, Hyperfine Interact. **9**, 87 (1981).
[27] A. Zemel and J. Dobes, Phys. Rev. C **27**, 2311 (1983).
[28] N. Yoshida, A. Arima, and T. Otsuka, Phys. Lett. B **114**, 86 (1982).
[29] Z. Y. Xu, Y. Lei, Y. M. Zhao, S. W. Xu, Y. X. Xie, and A. Arima, Phys. Rev. C **79**, 054315 (2009).
[30] J. B. Mcgrory and T. T. S. Kuo, Nucl. Phys. A **247**, 283 (1975).
[31] D. Zwarts and P. W. M. Glaudemans, Z. Phys. A **320**, 487 (1985).
[32] L. Coraggio, A. Covello, A. Gargano, N. Itaco, and T. T. S. Kuo, Phys. Rev. C **58**, 3346 (1998).
[33] L. Coraggio, A. Covello, A. Gargano, N. Itaco, and T. T. S. Kuo, Phys. Rev. C **60**, 064306 (1999).
[34] E. Caurier, M. Rejmund, and H. Grawe, Phys. Rev. C **67**, 054310 (2003).
[35] C. W. Ma and W. W. True, Phys. Rev. C **8**, 2313 (1973).
[36] T. R. McGoram, G. D. Dracoulis, A. P. Byrne, A. R. Poletti, and S. Bayer, Nucl. Phys. A **637**, 469 (1998).
[37] K. Higashiyama and N. Yoshinaga, EPJ Web of Conferences **66**, 02050 (2014).
[38] P. Walker and G. Dracoulis, Nature (London) **399**, 35 (1999).
[39] Evaluated Nuclear Structure Data File (ENSDF), www.nndc.bnl.gov/ensdf/.
[40] C. J. Chiara and F. G. Kondev, Nucl. Data Sheets **111**, 141 (2010).
[41] F. Kondev, Nucl. Data Sheets **109**, 1527 (2008).
[42] F. G. Kondev, Nucl. Data Sheets **105**, 1 (2005).
[43] F. Kondev, Nucl. Data Sheets **101**, 521 (2004).
[44] F. C. Zawislak and J. D. Bowman, Nucl. Phys. A **146**, 215 (1970).
[45] F. Kondev and S. Lalkovski, Nucl. Data Sheets **112**, 707 (2011).
[46] P. K. Hopke, R. A. Naumann, and K. H. Spejewski, Phys. Rev. **187**, 1709 (1969).
[47] G. Astner and M. Alpsten, Nucl. Phys. A **140**, 643 (1970).
[48] M. S. Basunia, Nucl. Data Sheets **121**, 561 (2014).
[49] J. Chena and F. G. Kondeva, Nucl. Data Sheets **126**, 373 (2015).
[50] B. Singh, D. Abriola, C. Baglin, V. Demetriou, and T. Johnson, Nucl. Data Sheets **114**, 661 (2013).
[51] I. Bergström, C. J. Herrlander, T. Lindblad, V. Rahkonen, K.-G. Rensfelt, and K. Westerberg, Z. Phys. A **273**, 291 (1975).
[52] E. Browne, Nucl. Data Sheets **104**, 427 (2005).
[53] M. S. Basunia, Nucl. Data Sheets **108**, 633 (2007).
[54] E. Recknagel, Y. Yamazaki, O. Hashimoto, S. Nagamiya, and K. Nakai, Phys. Lett. B **52**, 414 (1974).
[55] A. P. Byrne, G. D. Dracoulis, C. Fahlander, H. Hubel, A. R. Poletti, A. E. Stuchbery, J. Gerl, and R. F. Davie, Nucl. Phys. A **448**, 137 (1986).
[56] I. Talmi, *Simple Models of Complex Nuclei* (Harwood, Chur, 1993).
[57] T. Otsuka, R. Fujimoto, Y. Utsuno, B. A. Brown, M. Honma, and T. Mizusaki, Phys. Rev. Lett. **87**, 082502 (2001).
[58] T. Otsuka, T. Suzuki, R. Fujimoto, H. Grawe, and Y. Akaishi, Phys. Rev. Lett. **95**, 232502 (2005).
[59] T. Otsuka, T. Suzuki, M. Honma, Y. Utsuno, N. Tsunoda, K. Tsukiyama, and M. Hjorth-Jensen, Phys. Rev. Lett. **104**, 012501 (2010).
[60] K. Kaneko, T. Mizusaki, Y. Sun, and S. Tazaki, Phys. Rev. C **89**, 011302 (2014).
[61] A. Umeya and K. Muto, Phys. Rev. C **74**, 034330 (2006).

[62] N. Yoshinaga and K. Higashiyama, Eur. Phys. J. A **30**, 343 (2006).
[63] P. R. Sala, N. Blasi, G. LoBianco, A. Mazzoleni, R. Reinhardt, K. Schiffer, K. P. Schmittgen, G. Siems, and P. von Brentano, Nucl. Phys. A **531**, 383 (1991).
[64] T. Hayakawa, J. Lu, K. Furuno, K. Furutaka, T. Komatsubara, T. Shizuma, N. Hasimoto, T. Saitoh, M. Kidera, Y. Hatsukawa, and M. Oshima, Z. Phys. A **357**, 349 (1997).
[65] V. Kumar, P. Das, R. P. Singh, S. Muralithar, and R. K. Bhowmik, Eur. Phys. J. A **17**, 153 (2003).